The Effects of Wakes on the Available Wind Power During Curtailment

INCLUDING A CASE STUDY OF WESTERMEERWIND

A Literature Study by **M. P. C. (Marthijn) Bontekoning**

THE EFFECTS OF WAKES ON THE AVAILABLE WIND POWER DURING CURTAILMENT

INCLUDING A CASE STUDY OF WESTERMEERWIND

Literature Study / Specialization Project

in preparation for a Master Thesis

to obtain the degrees of Master of Science
Offshore Engineering and Dredging at the Delft University of Technology and
Technology-Wind Energy at the Norwegian Institute of Science and Technology

by

M. P. C. (Marthijn) Bontekoning

Student number	4100867 (TU Delft), 763394 (NTNU)	
Project duration	November 1st, 2015 – July 31st, 2016	(expected)
Thesis committee	Prof. dr G.J.W. van Bussel	TU Delft (chair holder)
	Dr ir M. Zaayer	TU Delft
	Mr. S. Sanchez, MSc.	TU Delft
	Prof. L. Sætran	NTNU
	Mr. J. Bartl, MSc.	NTNU
	Dr ir B. Ummels	Ventolines BV
	Ir A. Walvis	Ventolines BV

TU Delft NTNU Ventolines

PREFACE

This literature study forms the theoretical basis of the subsequent Master thesis. The Master thesis is part of the track Offshore Engineering of the European Wind Energy Master. It is written at the Delft University of Technology in the Netherlands in order obtain the degree of Offshore Engineering and Dredging, and at the Norwegian Institute of Science and Technology in order to obtain the degree of Technology-Wind Energy. As the two degrees have different requirements on a literature study, a hybrid form was found together with the supervisors. I would like to thank my supervisors Sebastian Sanchez and Michiel Zaayer from TU Delft and Jan Bartl and Lars Sætran from NTNU for being this flexible and for providing valuable literature references and feedback.

In collaboration with Ventolines BV, the wind farm Westermeerwind will be used as a case study to validate the theoretical and associated numerical methodology created in the Master thesis. Both Ardaan Walvis and Bart Ummels from Ventolines BV have helped me greatly with establishing this Thesis topic and getting me started with the right literature. I would therefore also like to thank them for supporting me. It is noted, however, that this report is written without any confidential information obtained from Ventolines BV and it can therefore be placed in the public domain completely.

Delft, The Netherlands
January 22^{nd}, 2016
Marthijn Peter Cornelis Bontekoning, BSc

TABLE OF CONTENTS

Preface v

1 Introduction 1
- 1.1 Wind Power Curtailment . . . 1
- 1.2 Wind Turbine Wakes . . . 2
- 1.3 Goal of this Report . . . 2
- 1.4 Outline Report . . . 3

2 Wind Power Curtailment 5
- 2.1 Reasons for Accurate Analysis of Curtailment . . . 5
  - 2.1.1 Surplus of Power in Grid . . . 6
  - 2.1.2 Overplanting a Wind Farm . . . 6
  - 2.1.3 Upward Power Reserve . . . 6
  - 2.1.4 Frequency Control Reserve . . . 7
- 2.2 The Business Case . . . 9
  - 2.2.1 Agreements with the TSO . . . 10
  - 2.2.2 Governmental Subsidies . . . 11
  - 2.2.3 Calculation Example . . . 12
- 2.3 Curtailment Mechanisms . . . 13
  - 2.3.1 Pitching . . . 13
  - 2.3.2 Overspeeding . . . 14
  - 2.3.3 Yawing . . . 15

3 Wind Turbine and Wake Fundamentals 17
- 3.1 Wake Fundamentals . . . 17
  - 3.1.1 Far and Near Wake Analyses . . . 18
  - 3.1.2 Vorticity and the Shear Layer . . . 19
  - 3.1.3 Effect of Turbulence Intensity . . . 20
  - 3.1.4 Axial Symmetry of the Wake . . . 22
  - 3.1.5 Wake Meandering . . . 24
  - 3.1.6 Yawed Flow . . . 24
- 3.2 Wake Interference . . . 25
  - 3.2.1 Lateral Wake Interference . . . 26
  - 3.2.2 Sequential Wake Interference . . . 26
- 3.3 Effect of Curtailment on the Wake Characteristics . . . 26
- 3.4 Effect of Wakes on the Available Power Estimators (APE) . . . 30
  - 3.4.1 APE . . . 30
  - 3.4.2 Example of Two turbines . . . 31

4 Wake Calculations & Models **33**
4.1 Engineering Wake Models . . . 33
4.1.1 N. O. Jensen . . . 34
4.1.2 Katic Correction for N. O. Jensen . . . 36
4.1.3 Choi and Shan Corrections for N. O. Jensen . . . 37
4.1.4 Ainslie . . . 40
4.1.5 G. C. Larsen . . . 41
4.1.6 S. Frandsen . . . 41
4.2 CFD Wake Models . . . 44
4.2.1 Navier-Stokes Equations . . . 44
4.2.2 Reynolds Averaged Navier-Stokes (RANS) . . . 45
4.2.3 Large Eddy Simulation (LES) . . . 46
4.2.4 A Concluding Remark on CFD . . . 47
4.3 Comparison Wake Models . . . 47
4.4 A Note on Software Packages . . . 47

5 Delineation of Scope & Outline Master Thesis **49**
5.1 Problem Statement . . . 49
5.2 Delineation of Scope . . . 50
5.2.1 Target Wind Farms . . . 50
5.2.2 Approach to Wake Modeling . . . 50
5.2.3 Power Estimation . . . 50
5.2.4 Approach Methodology . . . 51
5.3 Outline Master Thesis . . . 51
5.3.1 Subdivision Tasks . . . 51
5.3.2 Deadline . . . 51
5.3.3 Supervisors . . . 51

Nomenclature **53**

List of Figures **55**

List of Tables **57**

References **59**

Appendices

A Westermeerwind **65**
A.1 Wind Farm Cluster Windpark Noordoostpolder . . . 65
A.2 Wind Farm layout . . . 66
A.3 Wind Turbines . . . 66

B Wind Turbine Fundamentals **69**
B.1 Power Curve . . . 69
B.2 Aerodynamics of the Momentum Theory . . . 71
B.3 The Betz Limit . . . 74
B.4 Blade Element Momentum Method . . . 75
B.5 Aerodynamics of an Airfoil . . . 77

1

INTRODUCTION

The electricity market is currently experiencing a paradigm shift from a market dominated by generators running on fossil fuels, towards a more varied market with multiple renewable power sources. Wind power has become a very interesting power source over the last decades. Mostly because it is clean and sustainable, it has an unlimited energy reserve, it has political benefits with respect to the fossil fuel based systems and it is widely available. This increasing demand has lead to a significant increase of wind power integration in the electricity grid.

Notwithstanding the well-known benefits of these new sources, this paradigm shift poses new challenges which are not studied well enough yet. This lack of knowledge and experience introduces avoidable risk and cost. This report is a literature study, which acts as the foundation of a Master thesis that focuses on a better understanding of one of these new challenges, namely wind power curtailment.

1.1. Wind Power Curtailment

The challenges of wind power are mostly related to its intermittent characteristics and (partly) unpredictable power output. The focus of this report is a result of the later. Whereas in an electricity market dominated by fossil fuels it is relatively easy for the supply to follow the demand, in an electricity market with high penetration of renewable energy sources, this is a bigger challenge. Taking into account must-run requirements of fossil fuel generators, high wind conditions might lead to a threat of overproduction of electricity, causing a potential power imbalance. This threat leads to the requirement of wind farms to temporarily reduce their power production. This is referred to as wind power curtailment. Vice versa, when a conventional generator fails, it could be an opportunity for a wind farm to take over this production, when its default operating mode is with curtailment. The difference between this curtailed power output and the possible power generation of the wind farm without curtailment, is referred to as available power.

If wind power is to play a mature role in the electricity generation market, it will have to deliver other system services besides maintaining the power balance. [1] As will be

explained in this report, this means that wind turbines (and wind farms as a whole) need to be curtailed in default operation mode, just like conventional generators. Whereas the available power of conventional generators is easy to calculate (generally their maximum capacity), this is more complex for wind turbines, as the wind speed is not constant.

Most modern wind turbines are already able to perform this (wind power) curtailment at short notice. Also, they are already equipped with some form of an available power estimator (APE), which can describe the amount of curtailed power quite accurately. However, summing the individual amounts of curtailed power of all turbines in a wind farm does not lead to the total curtailed wind power, because the interference effects between turbines during curtailment also needs to be considered. [2] Therefore a need arises for an Available Farm Power Estimator (AFPE), which accurately calculates the total available power for a complete wind farm, taking into account these inter-turbine effects. The AFPE makes it possible to more accurately calculate the total amount of wind power that is being curtailed.

1.2. Wind Turbine Wakes

Modern wind turbines are currently able reach a rated power of $8MW$. [3] They are often placed in clusters forming wind farms of several hundreds of megawatts. Because these wind turbines are placed relatively close to each other in a wind farm, they influence each other. The most dominant inter-turbine effect are the wakes generated by the turbines.

In general the more power per area a wind turbine extracts from the wind, the higher the velocity drop across the rotor is, as a result of the conservation of energy. This reduction in wind speed is called the wake and it will die out over time and downstream distance as the wake interacts with the atmosphere as a result of the conservation of momentum. Placing a second turbine within about 10 times the diameter of the first turbine means that this wake will influence the second turbine. [4]

This effect is already studied extensively, but there is still a lot of debate about different methodologies to estimate this effect, as will be discussed in this report. The main parameters are the turbine dimensions, the wind speed, the wind direction in combination with the farm layout, the turbulence intensity and the curtailment. With the increasing size of turbines and a growing offshore wind market, which has a lower turbulence intensity, including the wakes in the AFPE evidently becomes more important.

1.3. Goal of this Report

Before the modeling of the wakes and their effect on the available power during curtailment can be studied, a solid knowledge is required about all the parameters that are at play. This report tries to describe as many theories and phenomena that are relevant to provide this knowledge in order to differentiate the major aspects regarding wakes during curtailment.

This report and its insights form the basis of a later Master thesis report. The purpose of the thesis is to develop a theoretical and associated numerical methodology for an AFPE. Because of the partnership with Ventolines BV, this numerical methodology can be validated against one of their wind farms, namely Westermeerwind. See appendix

A for more information about Westermeerwind. In the end of this report the necessary delineations of the found theories and phenomena that lead to the scope of the Master thesis will be determined.

1.4. Outline Report

In order to study the effects of wakes on the available wind power during curtailment, first a solid understanding of wind power curtailment is required. This will be discussed in chapter 2. This chapter will also discuss the reasons of curtailment, its business case and curtailment mechanisms in more detail. Second, the phenomena of wakes are studied in detail in chapter 3, including the interference between wakes of different turbines. As both major phenomena are now well understood, the effect of curtailment on wind turbine wakes can be studied as well. Chapter 4 will discuss different methodologies of estimating the wakes and their interference effects, using wake models from literature. Chapter 5 can be considered the conclusion of this report, in which the delineation of the scope and the outline of the following Master thesis will be determined.

2

WIND POWER CURTAILMENT

The Oxford dictionary defines curtailment as *the action or fact of reducing or restricting something*. Wind power curtailment can therefore be understood as reducing the output of a wind farm to a determined value, which is lower than the maximum capacity of that wind farm. In standard conditions a wind farm operator will exploit its assets at maximum financial optimum with respect to the wind conditions. This will practically result in maximizing the power production of the wind farm. In certain cases, however, reasons may arise that the operator wants or is required to limit this production to a sub-maximum level. In these cases the wind farm is considered to be curtailed, which leads to costs of opportunity loss, i.e. the loss in profit from production with respect to the available power. The wind power producer loses part of its projected revenue, which has an impact on the investment payback time. [5]

The reasons of curtailment come from different stakeholders of the wind farm and can be divided into two groups: normal downward curtailment and downward curtailment for upward reserves. From each of these groups, two reasons and their origin will be discussed in the first section. The second section will treat the business case related to the opportunity loss of curtailing wind power and the agreements with the Dutch grid or transmission system operator (TSO). Finally, when the decision to curtail the wind power is made, several mechanisms can be used to achieve this. It will be explained in the third section which mechanisms are favorable given the situation.

2.1. Reasons for Accurate Analysis of Curtailment

The demand of the analysis of the effect of curtailment come from the different reasons to curtail the output of the wind farm. These reasons come from different stakeholders of a wind farm. Two major stakeholders can be identified. The first stakeholder is the grid operator. It is his responsibility to balance the production and consumption of the grid and maintain its quality. The second stakeholder is the owner of the wind farm. His goal is to maximize the profit of the wind farm. When curtailing the output of a wind farm, it is important to know the exact amount of lost production. Also, the owner

might choose for maintaining a power reserve as a service to the grid operator if this is financially interesting. The following reasons for the accurate analysis of curtailment are defined. [6]

2.1.1. Surplus of Power in Grid

When the grid operator projects a surplus of power production with respect to either consumption or grid capacity, it can demand a curtailment of the output of a wind farm. The Danish grid operator Energinet.dk will demand this curtailment when either the security of supply is in danger or to secure an economic optimal use of the electricity supply system. The latter includes ensuring a functioning competitive market. [7] The definition of this functioning competitive market is open for debate and it is therefore a political decision to grant priority or not to wind farms with respect to fossil fuel based generators. Wind farms owners that are obligated to curtail their wind power will in many cases receive a compensation for their lost production. This will be treated in more detail in section 2.2.

An alternative of this curtailment is to sell the surplus to other connected grids. Although it would make sense to let the wind farms produce as much energy as possible, this is not always the case. A study from 2006 [8] found that the cost of avoiding the surplus was much lower than investing in high-voltage transmission lines. The rules and regulations about making this decision depend completely on the local laws.

2.1.2. Overplanting a Wind Farm

A second form of normal downwards curtailment can arise when designing a new farm. One of the design interfaces is the grid connection. Often there is a maximum amount of power that can be inserted into the grid. It is the challenge of the designer to optimize the use of the land/ocean area that is available. Therefore, the designer might choose to put an amount of wind turbines in its wind farm with a total rated power higher than the grid connection capacity. This is called overplanting or overbooking.

When the power curve will discussed in section B.1, it will be shown that there is a large region of wind speeds when this rated power is not produced. Overplanting results in higher energy yield at sub-rated (low wind speeds) production and therefore also a higher usage of the grid connection.

However, when the turbines are all operating at rated power (at high wind speeds), some of this power needs to be curtailed as it can not be exported to the grid, see figure 2.1. For the planning of the wind farm it is important to know how often this situation will occur and how much of the power is curtailed exactly. If this is known, a trade-off can be made to either invest in reinforcement of the grid connection or accept the loss production.

2.1.3. Upward Power Reserve

Nord Pool Spot is one such a power trading market for northern Europe. It consists of two types of markets. [10] The main market is the so called day-ahead market. In this market buyers and sellers of electricity meet and settle on a price. This is the market where the majority volume of the energy market is traded. Often, buyers and sellers also meet outside this market to place securities for a longer term.

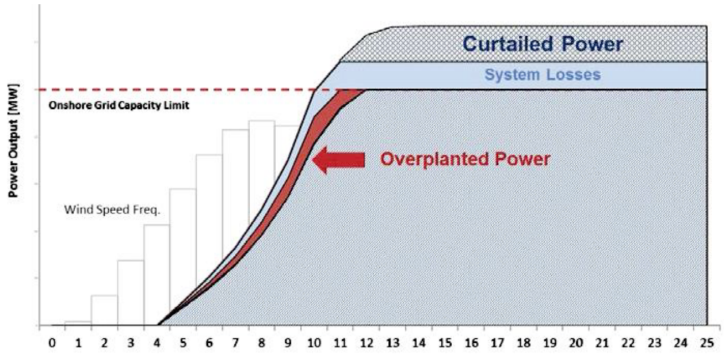

Figure 2.1: Power curve of a overplanted wind farm, showing the beneficial overplanted power and the lost curtailed power. The x-axis denotes the wind speed in $[\frac{m}{s}]$ [9]

The second market of Nord Pool Spot is the hour-ahead, or intraday, market is a more critical market in the sense that this is where the production and consumption can be balanced exactly. There are many reasons, why the trading on the day-ahead market does not guarantee this balance already. For example, when a nuclear power plant has to be shut down, a major imbalance is created and energy suppliers need to buy replacement power quickly. Also, when the wind is stronger than expected a surplus is created.

When a party is in direct need of power it has to pay a higher price at the hour-ahead market, than when this need is scheduled and can be bought on the day-ahead (or even month-ahead) market. Therefore, grid operators have reserve power contracts with energy producers. In these contracts a power producer agrees to have an overcapacity and reserve this capacity for the grid operator as a service. The grid operator can use this reserve for example in the mentioned case of a shut down of a nuclear power plant.

In order for a wind farm operator to make such a contract, it is important to know the exact amount of reserve the wind farm has at a certain level of curtailment. When the effect of wakes on the available power during curtailment is neglected, the overestimation will lead to a too high power reserve. When the grid operator appeals the available power and it is not enough, it might result in an outage or a very high price of buying additional power on the hour-ahead market.

2.1.4. Frequency Control Reserve

The last reason, although its technical details are outside the scope of this report, is the capacity to provide a control of the grid frequency. When the grid is overloaded, i.e. the power production is higher than the consumption, the frequency of the grid will drop as a result of this. An important task of the grid operator is to ensure that the deviation from the normal frequency (either $50Hz$ or $60Hz$) remains within a small band. This band is set by regulations as $0.04Hz$ in Europe. [11].

Several mechanisms are in place to make sure that in the case of a sudden drop or increase in production or consumption, the grid frequency stays within this defined band. These are referred to as inertial and active reserves. Inertial reserves are created by the actual rotating masses in classical synchronous generators. The strong coupling

between their rotational speed and the electrical frequency results in a passive counter force for sudden changes in the frequency in the grid. [12]

Active reserves are grouped in primary, secondary and tertiary reserves. The designation of an active reserve depends on the reaction time of the reserve. Primary reserves respond within several seconds to the event (maximum 30 seconds within ENTSO-E [13]). Secondary reserves have the capacity to react withing several minutes, relieving the primary reserves (after 15 minutes within ENTSO-E [13]). The primary reserves are able to react to new disturbances as soon as the secondary reserves are active. Whereas primary and secondary reserves need to be enabled automatically, tertiary frequency control reserves can be initiated manually as well. An example can be to fire up a generator that was offline before the event. These defnitions are taken from the glossary of the UCTE Operation Handbook[14] Figure 2.2 shows the mentioned consecutive frequency reserves.

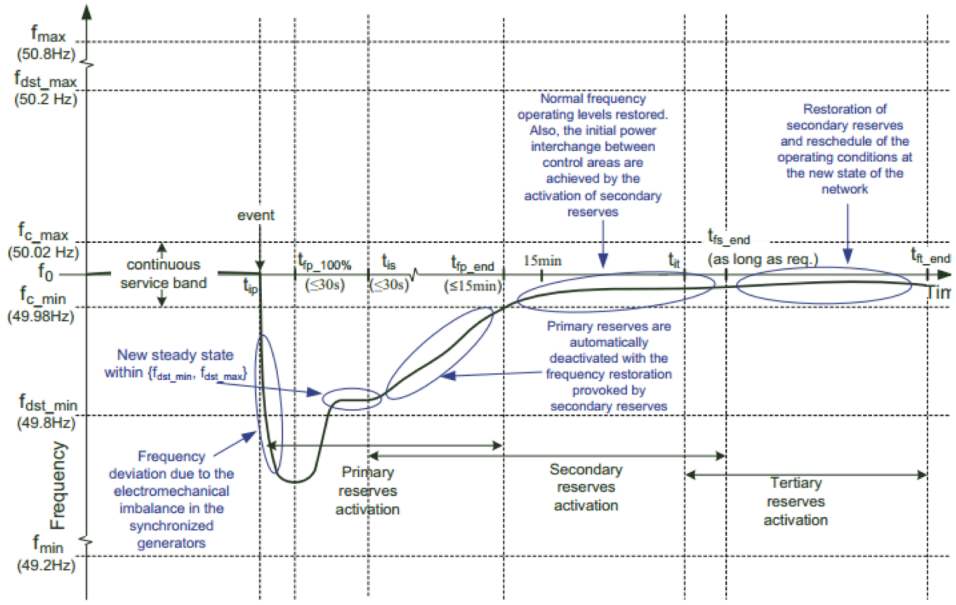

Figure 2.2: Primary, secondary and tertiary frequency control reserves [15]

Using the knowledge of a need for frequency control reserves, it is interesting to look how curtailment of wind turbines can help increase this capacity. Figure 2.3 shows two graphs for a wind farm that is not under curtailment. The upper graph shows the frequency in the grid (the different values of K_p and K_f are not of interest here). It shows that the wind farm is able to compensate for the sudden change in frequency as a primary reserve, but after a while a second dip occurs. A wind turbine that operates at rated power, can be overloaded for a short period for this, but after a while the temperature of the generator would rise too much and the turbine has to go back to nominal. This results in the visible second dip and disqualifies this wind farm for a secondary reserve

possibility.

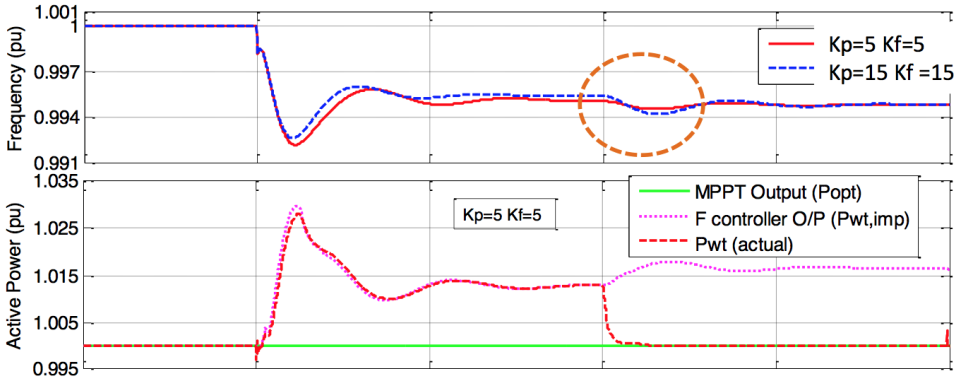

Figure 2.3: Stabilizing capacity of a wind farm without curtailment. [15]

Figure 2.4 shows the same kind of graphs as in figure 2.3, but with a 5% curtailed wind farm. The second dip does not occur in this case, as the turbine is able to keep producing at this higher level indefinitely, as it is still sub-rated. This wind farm can therefore qualify as both a primary and secondary power reserve. As the wind power market keeps on maturing and is being integrated more and more, it becomes more important to analyze the power available for upward reserves to control the grid frequency. [16]

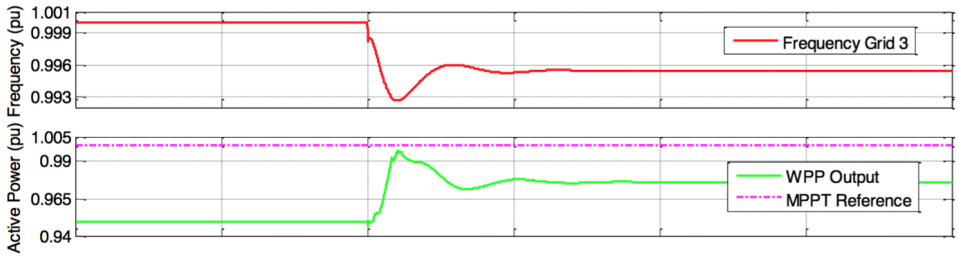

Figure 2.4: Stabilizing capacity of a wind farm being curtailed for 5% curtailment. [15]

2.2. The Business Case

Now that all reasons for curtailment are identified, it is interesting to look at the impact of curtailment on the business behind operating a wind farm. It has to be noted that this impact is very dependent on the laws and regulations that act on the wind farm. This section is modulated to the business case of the wind farm Westermeerwind in The Netherlands, see appendix A for more information on the wind farm.

2.2.1. Agreements with the TSO

In The Netherlands there are no agreements between the grid operator and wind farm operators with respect to the primary reserve.

For the secondary reserves a different system applies. Entities that submit either generation or load schedules are referred to as a power responsible party or PRP. The Dutch TSO TenneT charges these responsible parties a certain price if they deviate from their schedule. However, when the deviation contributes to the balance of the system they will be paid that price instead. [13]

All big market parties are assigned such responsibilities and need to have handed in their schedules at 12 AM for the next day, with a resolution of 15 minutes (referred to as a programe time unit or PTU). (The Danish TSO Energinet.dk requires a 5 minute resolution for offshore wind farms [7].) This allows TenneT to buy in the necessary expected power to maintain balance from the primary and secondary power reserves (see section 2.1.4 for these definitions). The costs resulting from this necessity are charged to the responsible parties. This is an incentive for the responsible parties to stick to their schedule. [8]

When the TSO notices a power imbalance in a 15 minute segment it is responsible to solve it. Two situations can be identified. Firstly, a surplus can expected and the TSO will ask the responsible parties to curtail their power. Secondly, when a shortage is expected, it will approach the responsible parties to ramp up their production. For wind turbines the latter is only possible when they were initially in curtailed conditions as explained in section 2.1.4. Figure 2.5 shows the settled imbalance of TenneT of the last week of 2015. This data can publicly be obtained from the website of TenneT[17] and is updated every 15 minutes. The shown volume is the net value, which refers to a surplus when it is possitive, but to a shortage when it is negative (only the surplus is shown here, for visualization or the calculation of section 2.2.3).

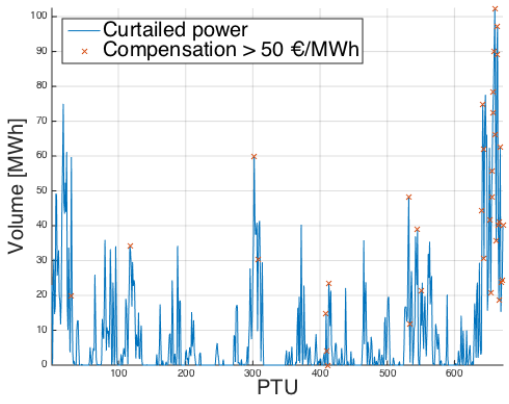

Figure 2.5: Settled imbalance of Dutch TSO TenneT. The red crosses indicate settlements with a price higher than €50 $\frac{€}{MWh}$ [17]

In order to solve the imbalance TenneT uses a bidding ladder to determine from

which party it buys or sells the required amount. All parties must have submitted their bids 14:45 hour. When the bids are accepted they cannot be withdrawn. TenneT will accept all bids it needs starting from the financially most intersting, i.e. lowest price when buying and highest price when selling. However, there is only one price per PTU. [18] This is determined to be the price that is the least favorable for TenneT, e.g. the highest buying price of all bids. The exact price is always determined after the PTU is finished. For the algorithm used, the reader is referred to [19].

In figure 2.6 the settled prices for the same week as figure 2.5 can be seen. A positive value for the upward adjustment means that TenneT pays the responsible party (i.e. Tennet buys energy while in shortage), while a negative value means that the responsible party pays TenneT (i.e. a PRP produces more energy than scheduled). For the downward adjustment (positive means PRP reduces power) this is the other way around. Considering wind power curtailment, a wind farm operator opens the opportunity for this upward adjustment when it sets it wind farm in permanent curtailment. The downward adjust is always possible and purpose of the Master thesis is the determine how much a wind farm is exactly curtailing with respect to the available power.

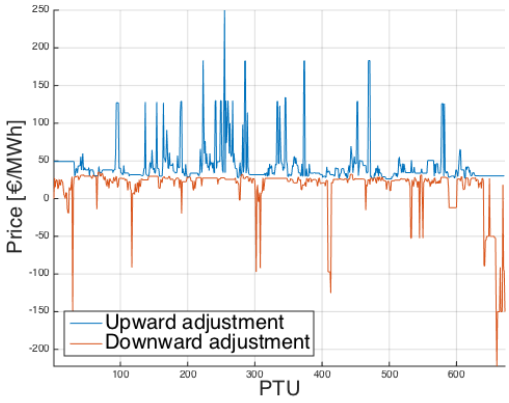

Figure 2.6: Settled prices for imbalance of Dutch TSO TenneT. The X-axis shows the time since December 19^{th}, 2015 at 00:00 in program time units (PTU) in 15 minutes for one week. [20]

2.2.2. Governmental Subsidies

Another important aspect with respect to the business case of wind power curtailment is the regulations for the governmental subsidies for wind energy. In The Netherlands the government uses a feed-in tariff. This means that the wind farm operator is subsidized the difference of the cost of energy (in $\frac{€}{MWh}$) with respect to a predefined base price. This value of this base price is dependent on the location of the wind farm and the type of location, e.g. onshore or offshore. The former dependency used to be based on the municipality of the wind farm, but from 2016 it depends on the exact coordinates through a government issued tool, called the SDE+ Windviewer. However, the exact amount of the subsidy can only be determined in hindsight as it also depends on the energy prices on the market.

2.2.3. Calculation Example

With respect to the business case of wind power curtailment it is only interesting for a wind farm operator to reduce the power of its wind farm when the compensation that it gets from the TSO is higher than the subsidy. For example, when a wind farm operator gets (an extremely high) subsidy of $250\frac{€}{MWh}$ there was no incentive to curtail the wind power when looking at figure 2.6 in that week. The maximum observed compensation for downwards adjustment was $222,40\frac{€}{MWh}$.

Using the data provided by the Dutch governmental organization Netherlands Enterprise Agency [21], a value of $€50\frac{€}{MWh}$ looks like a more realistic subsidy for Westermeerwind (this value was not confirmed by Ventolines BV). This would lead to an additional profit of $172,40\frac{€}{MWh}$ when the operator curtails its production. It now becomes very clear why it is important to know exactly how much power is being curtailed by wind farms as this determines the eventual compensation.

In the week of figure 2.6 there are 36 PTUs with a price lower than $-50\frac{€}{MWh}$ (referred to as interesting PTUs or iPTUs), meaning that the wind farm could have been curtailed for 9 hours (5% of the whole week). In figure 2.5 the volumes with a compensation higher than $€50\frac{€}{MWh}$ are indicated. The total curtailed power in The Netherlands with compensation higher than $€50\frac{€}{MWh}$ that week was $1,568MWh$ with a total cost of for TenneT of €170,000. These same values have been calculated for the last few years in order to indicate the size of the potential, see table 2.1. *Amount iPTUs* refers to the amount of PTUs that have a price higher than $€50\frac{€}{MWh}$. *Market size iPTUs* is the total volume of these iPTUs times their individual price.

Figure 2.7 shows the trend of the market size from table 2.1 indicating that the interesting part of the curtailment market for wind turbines has increased of the last few years. This means that it becomes more interesting for a wind farm operator to make some the capacity of the wind farm available for this reserve in order to profit from this market.

Table 2.1: Overview of market size power curtailment for last few years [17][20]

Year	Amount iPTUs	Volume iPTUs	Market size iPTUs	Average price iPTUs
2015	6%	53 GWh	$7.0M€$	$132\frac{€}{MWh}$
2014	3%	27 GWh	$3.5M€$	$130\frac{€}{MWh}$
2013	5%	37 GWh	$6.2M€$	$168\frac{€}{MWh}$
2012	5%	43 GWh	$5.5M€$	$128\frac{€}{MWh}$
2011	4%	33 GWh	$4.0M€$	$121\frac{€}{MWh}$
2010	1%	12 GWh	$1.5M€$	$126\frac{€}{MWh}$
2009	2%	20 GWh	$2.6M€$	$130\frac{€}{MWh}$
2008	<1%	1 GWh	$0.2M€$	$125\frac{€}{MWh}$

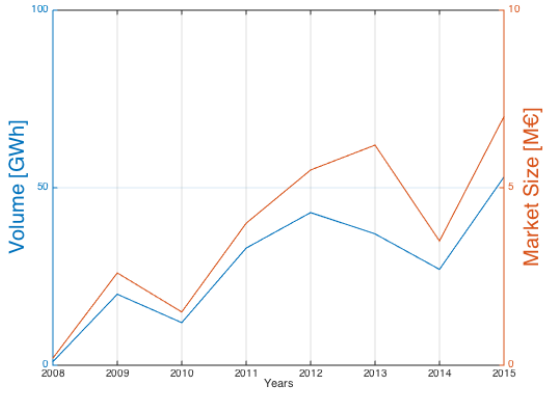

Figure 2.7: Increase in market growth of interesting part of power curtailment market for wind turbines (compensation higher than 50 $\frac{€}{MWh}$), see table 2.1 [17][20]

A last note is made, that although it is not happening now, in the future the TSO could pay a wind farm for offering the service of curtailment for upward reserve. This will shift the trade-off of the wind farm operator towards permanent curtailment.

2.3. Curtailment Mechanisms

Now that the reasons of curtailment have been defined and the economical incentive is also clear, it is interesting to look at the technical mechanisms to achieve curtailment. These mechanisms can be divided into two types. In the first type complete turbines are being shut down. For example, given a wind farm consists of 100 turbines. Shutting down 10 turbines will lead to a curtailment of 10% (without taking the wake effects into account).

The second type, which is the type of curtailment mechanism that is treated in this report, is to curtail each turbine at an individual level. So in order to achieve the same 10% curtailment as in the previous example and again without taking into account the wake effects (see next section), each turbine has to be curtailed 10% itself.

2.3.1. Pitching

Pitching of the blades leads to a decrease in power. This mechanism is already ensuring that the generator will not get overloaded, as will be explained in more detail in section B.1. The same aerodynamic principle can be used before rated power, in order to curtail the wind power.

An increase in the pitch angle, will lead to a lower power production. Figure 2.8 shows the effect of changing the pitch angle on the power output of the turbine. While applying the pitching mechanism, the rotor speed is kept constant, so the power production will drop from A to B. [11]

From figure 2.9 the required pitch angle can be determined at a given wind speed for a $2MW$ wind turbine from [22]. It can be seen that for high wind speeds only a small

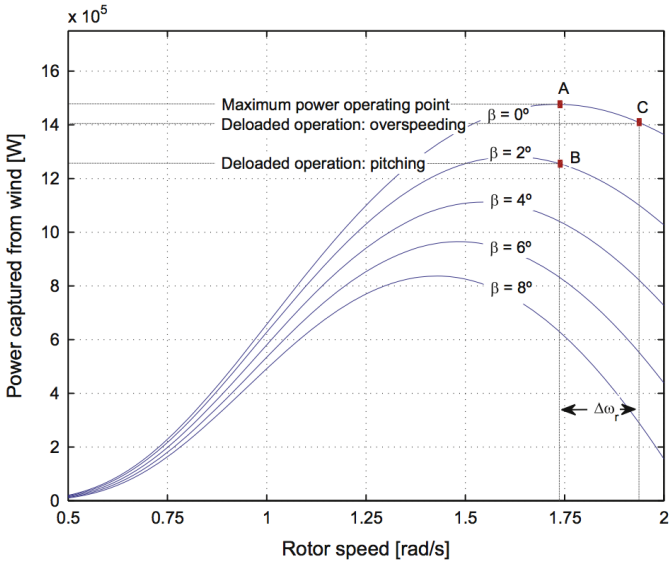

Figure 2.8: Curtailment mechanisms B pitching (pitch angle β) and C overspeeding ($\Delta\omega_r$) compared to default operation A [11]

change in pitch angle, can reduce the power output significantly. For example, to go from the red line to the blue line at a wind speed of $20\frac{m}{s}$ only needs a change in pitch angle of 0.6^o for this turbine model. But the required pitch angle for controlling the power at lower wind speeds has rather large variations, e.g. 9^o at $8\frac{m}{s}$. This is a cause for wear of the pitching mechanism. Another mechanism, namely overspeeding, is therefore preferred in the low wind speed range. Sometimes, three regions are defined, where the middle region is a combination of pitching and overspeeding. [11].

2.3.2. Overspeeding

The second common method of wind power curtailment is to allow the rotor to speed to increase above its optimal point. Figure 2.8 shows that when the rotor speed is increased from the optimal value of $1.7\frac{rad}{s}$ at point A to $1.9\frac{rad}{s}$ at point B, the power is reduced from $1.5MW$ to $1.4MW$ when the pitch angle is kept constant. It is also possible to achieve the curtailment with a reduction of rotor speed, i.e. setting the rotor speed to $1.5\frac{rad}{s}$ in figure 2.8, but this a less favorable option. In the transient of decreasing the rotor speed, the rotor will release kinetic energy and thus the power generation will temporary increase. Considering the importance of a primary frequency reserve as mentioned before, a destabilizing transient of a control mechanism is considered detrimental.

Figure 2.10 is analogous to figure 2.9. It shows the required rotor speed for different amounts of curtailed wind power. Only lower wind speeds are shown, as for higher wind speeds pitching is the preferred mechanism.

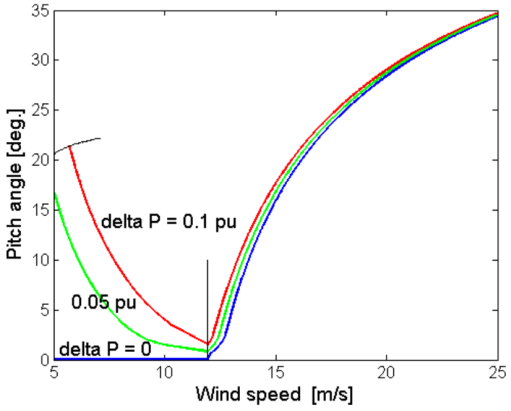

Figure 2.9: Required pitch angles for different amount of curtailments (delta P) depending on the wind speed. [22]

2.3.3. Yawing

A third mechanism is yawing the rotor out of the wind from its optimal point. When looking at the effect of yawing on the power coefficient there is, however, much more debate than with the previous two methods.

From [23] it is found that the expression of the power coefficient has to be altered, as well as the expression for the optimal induction factor, see equations 2.1 and 2.2 [23]. This leads to a dependency of the optimal power coefficient on the cosine of the yaw angle with a cubic relation. However experimental results suggest a quadratic relation [24][25], while other models conclude that it depends on the specific case (e.g. number of blades) and neither a quadratic nor a cubic relation is representative[26]. Figure 2.11 is a possible qualitative representation of dependency of the power coefficient on the induction factor while yawing, when taking the cosine cubed. It shows that a relatively big yaw angle is required before significant power reduction occurs. The mentioned decreasing maxima of the curves can bee seen as well.

$$a = \frac{\cos(\gamma)}{3} \tag{2.1}$$

$$C_P = 4a(\cos(\gamma) - a)^2 \rightarrow C_{P_{opt}} = \frac{16}{27}\cos^3(\gamma) \tag{2.2}$$

When the turbine is in yawed position the blades of the rotor endure a considerable extra cyclic load due to the in-plane velocity component, namely $V_0 \sin(\gamma)$, see section 3.1.6 for an elaboration on this. Combined with the fact that yawing is generally slower than pitching or overspeeding and the inconclusive literature on the mathematical expression of its effect on the turbine loading, it is not further considered as an interesting curtailment mechanism for this analysis.

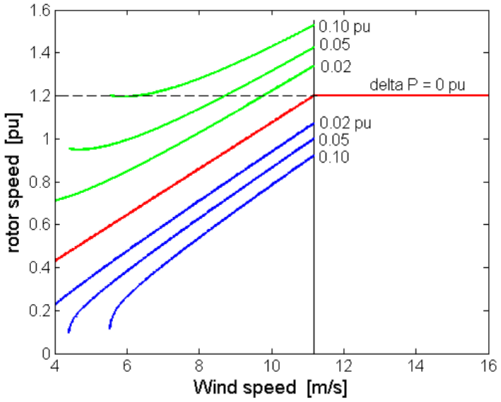

Figure 2.10: Required rotor speeds for different amount of curtailments (delta P) depending on the wind speed. [22]

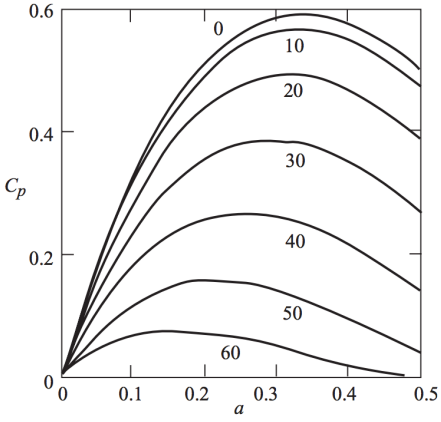

Figure 2.11: Required yaw angles for different amount of curtailments depending on the induction factor. [22]

3

Wind Turbine and Wake Fundamentals

Although historically wind energy harvesting machines were used for grinding grain, pumping water for irrigation or even preventing the sea from flooding The Netherlands, the main purpose of a wind turbine today is generating electricity. [27] This process can be subdivided into two consecutive conversions. First, the kinetic energy of the moving air mass is converted to rotational mechanical energy of the turbine's main shaft. Second, this mechanical energy is converted to electrical energy, using a generator. [28]

Wakes and all their consequences, are a result of the first conversion. In this process the interaction of the turbine blades with the moving fluid are key. This interaction results in the required torque to pass on to the generator. By extracting this kinetic energy from the wind, there will be an unavoidable velocity deficit directly behind the rotor. The fluid with the velocity deficit will continuously mix with the surrounding fluid. This leads to a gradual dissipation of the wake.

This chapter consist of three parts. Before the wake itself can be discussed, it is important to have some fundamental knowledge of the wind turbine first, as this is where the wakes originate from. The reader is referred to appendix B for this required knowledge and references to further literature. In the first section the general concepts and characteristics of wakes are discussed. The second section will use this knowledge to better understand the interference of wakes in a wind farm. Finally, this chapter will be stitched together with the previous chapter, by analyzing the effect of curtailment on the wake characteristics.

3.1. Wake Fundamentals

Now that the low level aerodynamics of the rotor are discussed, it is time to look at the wake it creates. It should now be obvious, that it is impossible to completely mitigate the wake behind the turbine. The energy used to rotate the rotor of the wind turbine is in direct relation of the amount of energy extracted from the wind. This leads to a

local energy deficit and therefore a wind speed deficit behind the rotor. This section will set out some main fundamentals of wakes and presents some conclusions that can be drawn from literature.

3.1.1. Far and Near Wake Analyses

First of all, it is important to make a clear difference in far and near wake characteristics. The transition area of these regimes can be assumed to be at $3D$ (three rotor diameters) downstream of the rotor. [29]. In the near wake, rotor (aero)dynamics play an important role. Parameters treated before, like the amount of blades, the airfoil and local stalling behaviour determine the properties of the wake.

As this report focuses on the effects of wakes on the available wind power of the whole wind farm, more attention will be payed to the far wake. In the far wake, the rotor and its blades are less important and the velocity profile has a Gaussian-like profile. See figure 3.1 for a repeated alteration of the near and far wakes behind five turbines. In the far wake more effort is put into analyzing the wake interference, turbulence models and selecting the right wake models. This allows for a deeper understanding of the mutual influence of turbines in a wind farm. The near wake, however, is relevant to some extent as it provides a form of initial conditions for the far wake.

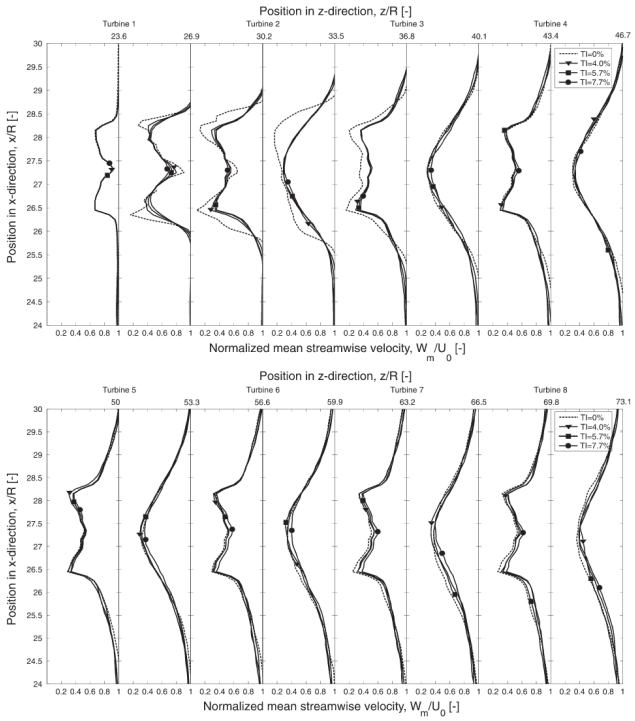

Figure 3.1: Alternation of near and far wakes behind five consecutive turbines [30]

3.1.2. Vorticity and the Shear Layer

The actuator disk theory, presented in section B.2 made the assumption that there is no rotation in the wake in order to simplify the BEM algorithm. The correction by Glauert [31] was mentioned to increase the accuracy of the algorithm. As this report moves away from rotor design and looks more into the wakes that are a result of this design, it becomes very important to look at this vorticy. Therefore, this shall section discard the assumption of zero rotation in the wake completely and look at the consequences of this vorticity on the wake.

Figure 3.2 shows the definition of the shear layer of the wake. In figure B.3 in the section about the actuator disk theory, the wind velocity changes abruptly from u_1 in A_1 to V_0 outside of A_1 over the outer streamline. Figure 3.2, however, shows a shear layer where this change is more gradual. The shear layer separates the slower moving fluid inside the wake from the fluid untouched by the rotor and contains a lot of defects. Neglecting this shear layer for blade design might be appropriate, but not for wake analyses, as this layer plays an important role for the incoming wind of a next wind turbine.

The shear layer originates from the shedded vortex sheets from the trailing edge of the blades, as mentioned in section B.5 about flow separation. These vortex sheets roll up and form tip vortices in helical trajectories, which can be approximated by the mentioned shear layer of figure 3.2.

The fluid inside the shear layer is made up of concentrated vortici and has a lower velocity and contains more defects than the atmospheric fluid outside the shear layer. The defects of the axial velocity are related to the axial thrust of the wind turbine, while the defects in the azimuth direction are related to the torque of the turbine. [32]

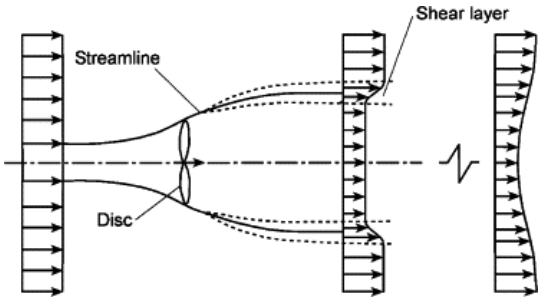

Figure 3.2: The shear layer of the actuator disk as a result of the vorticity in the wake [32]

The ring-shaped shear layer, where the velocity gradient is rather high, can be well-observed. The velocity gradient inside the shear layer, leads to the generation of new turbulent eddies and a higher corresponding turbulence intensity. Due to turbulence diffusion, the thickness of this shear layer increases with downstream distance, see figure 3.3.

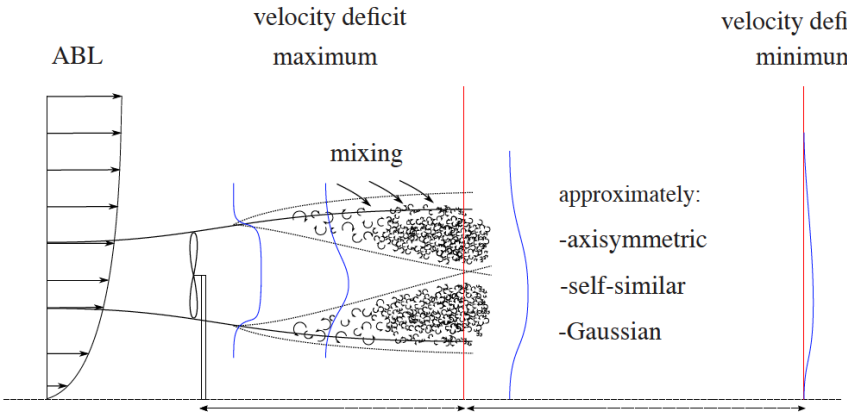

Figure 3.3: Shear layer developing with distance [33]

3.1.3. Effect of Turbulence Intensity

The turbulence intensity (TI) is defined as in equation 3.1, where σ_u and μ_u are the standard deviation and mean of the wind speed.

$$TI = \frac{\sigma_u}{\mu_u} \tag{3.1}$$

Atmospheric Turbulence

Turbulence can be understood as a very chaotic type of flow. This random motion causes mixing of the flow with its surrounding flow and transfers the momentum of the flow outside of the wake into the wake. This leads to an expansion of the chaotic flow (i.e. the wake), but in a weaker form with a reduced velocity deficit. This process is called turbulent diffusion. Characteristic values for the turbulence intensity in the atmospheric flow typically range from 10% to 20% [34]. As the interaction with the ground is a cause of turbulence creation, offshore environments generally have a lower turbulence intensity.

Many studies [35] have indeed shown that an increase in the turbulence intensity of the incoming wind, reduces the time (and corresponding distance) before the wake can be considered to be dissipated. Figure 3.4 from Holzäpfel [35], shows the decay of the wake against the non-dimensional time, based on the computational expensive Large Eddy Simulations (LES). The attention is drawn to the comparison of the low turbulence (5.5%) and high turbulence (24%) of both the single vortices (SV) and vortex pairs (VP), e.g. $HIT\ SV_{5,5\%}$, $HIT\ VP_{5,5\%}$ and $HIT\ SV_{24\%}$, $HIT\ VP_{24\%}$, respectively. The figure also shows the effect of atmospheric stratification and the presence of shear flow, which are not treated now.

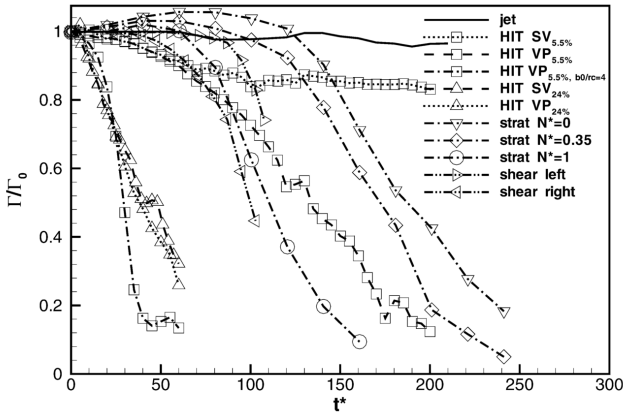

Figure 3.4: Effect of turbulence intensity, shear and stratification on the vortex decay of a single vortex (SV) and a vortex pair (VP) as a function of the non-dimensional time[35]

Added Turbulence

Just as the interaction with the ground causes turbulence, each turbine introduces additional turbulence to the flow, see figure 3.5. This is referred to as turbine induced turbulence or added turbulence. The causes include the friction stress between the blade surface and the wind, the break down of the tip vortices and wake meandering. [36] See section 3.1.5 for more information on the latter.

The figure shows the first three turbines in an array. There is a major difference in the areas behind these three turbines. Where the first area follows an almost laminar flow of the tip vortices, the second area visualizes the added turbulence clearly and the third area even more. The increase in the total added turbulence of all upstream turbines is at one point in balance with the momentum exchange with the ambient flow.

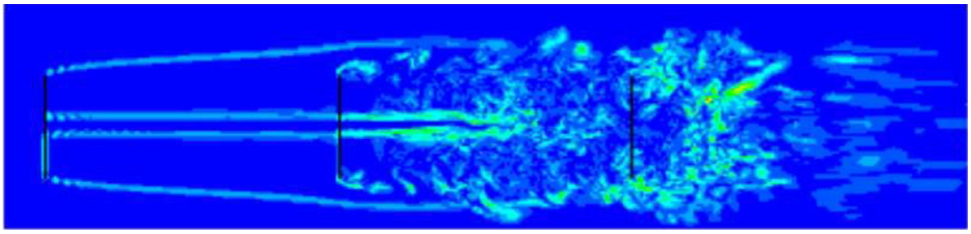

Figure 3.5: A visualization of added turbulence [4]

Figure 3.6 shows a measured proof of the added turbulence. It is measured at the Middelgrunden wind farm, in which the turbines are installed in an almost straight line from North to South. At these directions (0° and 180°), the turbulence intensity is significantly increased for a turbine standing for a turbine in standing in the middle of the wind farm. Barthelmie et al. [37] report an increase of 14% in the turbulence intensity of this specific case.

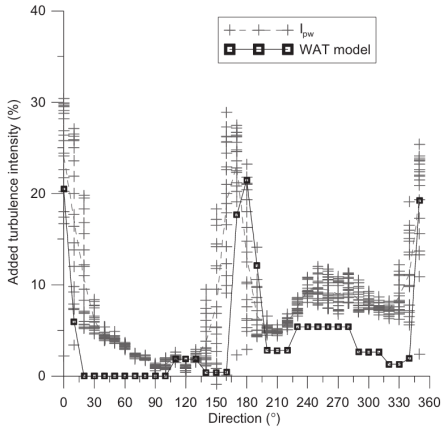

Figure 3.6: Added turbulence due to neighboring turbines standing at 0° and 180° for the Middelgrunden wind farm. The values I_{pw} are from measurements, while the values of the WAT model are for a model discussed in the article.[37]

3.1.4. Axial Symmetry of the Wake

Until now, the wake is assumed to grow symmetrically with respect to the rotor axis. There are, however, a couple of phenomena that invalidate this assumption. In reality, the point of maximum velocity deficit is slightly under the axis, while the point of maximum turbulence is slightly above the axis. [33]

Wind Shear

The uniform flow of the atmosphere is another important assumption which is not valid in the original actuator disk theory. The incoming wind is not uniform, but follows a so called wind shear, due to friction with the ground. Commonly, a power law wind profile is assumed for models, as in equation 3.2, where m is a coefficient called the shear component. The value of m is generally in te range of 0.1 and 0.25. [27] This wind shear leads to a higher wind speed in the upper section of the wake. Therefore, the wake rotates downwards, as can be seen in figure 3.7. Local effects due to the self-induced velocity however cause an overall upward shift of the wake structure. [38]

$$u(z) = u_{hub}\left(\frac{z}{z_{hub}}\right)^{m} \tag{3.2}$$

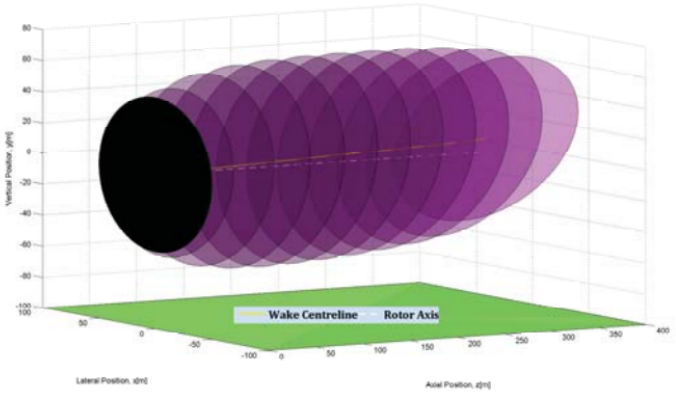

Figure 3.7: Wake visualization of sheared flow. [38]

Ground Boundary

As already mentioned before, besides the turbulence intensity, also the ground has an effect on the growth of the wake. [39]. The shear layer of the wake expands and at one point it will come close to the ground. The ground acts as a physical unmovable boundary. This expansion of the wake therefore loses its axial symmetry, as there is no physical boundary at the top. For offshore wind turbines this effect might be bigger, as they tend to have a lower hub height than onshore turbines.

From [38] it appears that the effects of the in ground effect are similar to the wind shear effect, but in the opposite direction. The ground accelerates the flow in the lower section of the wake more than in the upper section of the wake. This, in turn, leads to a rotation upwards. The same local effects due to self-induced velocity apply, causing an downwards shift of the wake structure.

In figure 3.8 the effect of the hub height and the thrust coefficient can be seen. As expected, an decrease in hub height and an increase in thrust coefficient, increases the in ground effect.

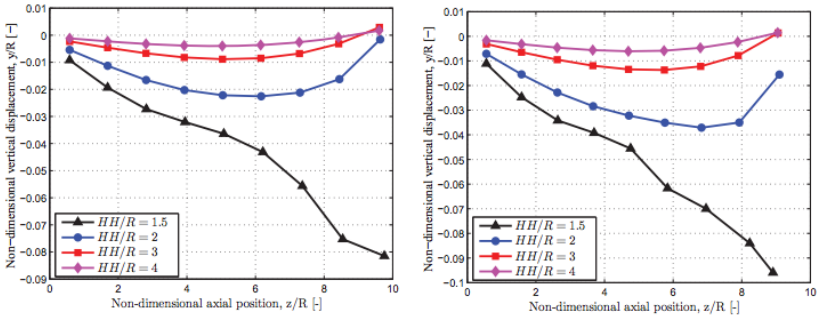

Figure 3.8: Influence hub height and thrust coefficient on the vertical shift of the in ground effect. The left graph is for a thrust coefficient of 0.64, while the right graph is for a thrust coefficident of 0.89. [38]

3.1.5. Wake Meandering

Besides the turbulence, most of the discussed wake fundamentals did not treat any unsteadiness of the incoming flow. However, both the wind speed and the wind direction are not constant over time. Unsteadiness due to the latter reason leads to meandering of the wake, i.e. the wake follows a sinusoidal shape downstream of the turbine as in figure 3.9

The low-frequency turbulence (large eddies) leading to large scale movement are not the only source of wake meandering. In the pragmatic approach of Larsen et al. [40] it is mentioned that the variability in wind direction is influenced by eddies of all sizes. Larsen also states that wake meandering of the wake increases the turbulence intensity. This is due to the increase of fluctuation in the wind speed at downstream turbines. Because of the wake meandering they can be fully in the wake, but also fully outside of the wake within relatively short periods. Therefore, wake meandering can be considered to have a positive effect on the dissipation of the wake.

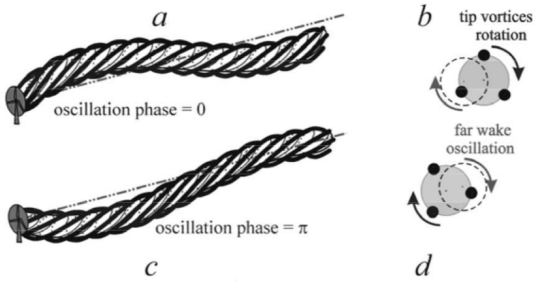

Figure 3.9: Visualizations of wake meandering [4]

3.1.6. Yawed Flow

As mentioned in section 2.3.3, yawing the rotor out of its optimal perpendicularity with the wind has a some drawbacks. Mainly with respect to the added cyclic loading due to the blades alternating in moving with versus against the wind. Figure 2.11 showed that a significant yaw angle is required to reduce the output power of the turbine. However, with a yaw angle of 20°, the lateral wind velocity on the rotor has already reached $V_0 \sin(20°) \approx 34\% V_0$.

This lateral component of the wind vector also has an effect on the direction of the thrust force. As was established before, the thrust force is the main force acting on the control volume of the wind. Therefore it can be concluded that, if the direction of that force is changed, the direction of the outgoing momentum also has to change.

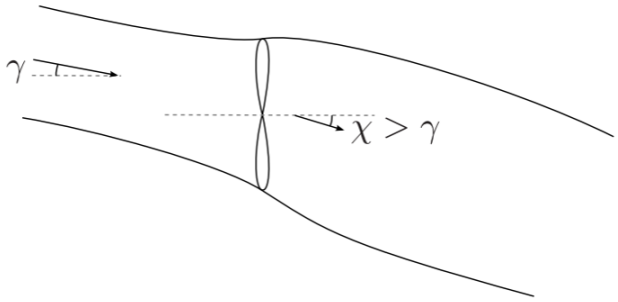

Figure 3.10: Wake angle due to yawed incoming flow [33]

Figure 3.10 shows that an incoming wind speed γ results in a wake skew angle χ. The wind turbine only extracts wind energy in the perpendicular direction of the rotor. This leads to the fact that the wake skew angle has to be bigger than the yaw angle. ECN holds a patent which it refers to as Controlling Wind [41] in which it defines the wake skew angle as in equation 3.3. This equation is derived and confirmed by [23]. The goal of Controlling Wind is to increase the total farm production by redirecting the wakes between the downstream wind turbines, instead of at the downstream turbine.

$$\chi = (0.6a + 1)\gamma \quad for \quad a = a_{opt} = \frac{1}{3} \quad \chi = 1.2\gamma \tag{3.3}$$

Wagenaar et al. [42] also define two other equations based on wind tunnel measurements (equation 3.4) and an LES model (equation 3.5). However, it concludes that although the results look promising in the performed experiments no significant effect of the controlling wind principle can be observed due to too much scatter in the data. It is therefor not further considered for this literature study.

$$\chi = (0.3C_T + 1)\gamma \quad for \quad C_T = C_{T_{opt}} = \frac{8}{9} \quad \chi = 1.27\gamma \tag{3.4}$$

$$\chi = 1.222\gamma \tag{3.5}$$

3.2. Wake Interference

Prior to this section, all turbines and their wakes were assumed to be isolated. However, as mentioned in the introduction, when looking for the Available Farm Power Estimator (AFPE), the interference between turbines and their wakes need to be looked at. As the actual calculation of the effect of wake interference is very complex, much depends on the selection of the wake model, described in chapter 4. This section will only discuss the wake interference on an theoretical level.

It is the wake interference that plays an important role in the design of the layout of a wind farm. As we will see in the next two subsections, wind turbine spacing plays an important role in the severity of the interference. One could argue that a bigger spacing will always lead to a better performance of a wind farm. Although this is true to some

extent, more forces act on the success of a wind farm. For example, most often there will be a limited amount of area available to build the wind farm. The goal is to extract the most energy at the best price, meaning that it could sometimes make sense financially to place more turbines in a fixed area, resulting in turbines standing in each others wake. Also, the electrical infrastructure can have a negative effect on the cost, when turbines are spaced far away from each other. The cables, required to connect to turbines to each other, need to be longer. [43]

There are two types of wake interference. The first wake interference is between two turbines standing next to each other with respect to the wind direction. Their wakes will come in contact with each other downstream of the wind. It is assumed, that this will occur in the far wake only, i.e. the lateral turbine spacing is big enough to let the near wakes develop independently. The second wake interference is the downstream interference between two sequential turbines.

3.2.1. Lateral Wake Interference

Because wakes dissipate by moving the momentum of the atmospheric flow outside the wake, with the slower moving fluid in the wake, the wake naturally expands.Therefore, when the wakes of two neighboring turbines meet, they can only expand in vertical direction as that is the only direction where atmospheric flow (and thus momentum) is available. [44]

3.2.2. Sequential Wake Interference

On of the assumptions of the actuator disk theory of section B.2 was a uniform incoming flow. It was already shown that due to the wind shear, this is not the case. For a wind turbine standing in the wake of an other upstream wind turbine, this becomes even more obvious. Both the turbulence intensity and the velocity deficit created by the upstream turbine form an input for the downstream turbine.

In reality, the wind direction will seldom be directly in line with the turbine layout. Therefore, it will be likely that only part of the upstream wake will hit the downstream turbine, making the analysis even more challenging. In a blind test, the impact of this offset on the wake of the downstream turbine was investigated. It was concluded that this wake is indeed much more complex than an individual wake. [45] Because of this complexity most wake analysis models use rotor averaging, using the momentum conservation to create a single value of the incoming velocity u_{rotor}, as in equation 3.6. [46]

$$(V_0 - u_{rotor})^2 = \frac{1}{A}\int_{rotor} (V_0 - u_w)^2 \, dA \tag{3.6}$$

3.3. Effect of Curtailment on the Wake Characteristics

As discussed in the introduction of this chapter, the velocity deficit behind a turbine is directly related to the amount of kinetic energy extracted from the wind. The power coefficient, defined in equation B.15, describes how much of this total kinetic power is extracted by the turbine. The important parameter, relating this power extraction to the velocity deficit is the induction factor a.

Another parameter that is directly related to the induction factor is the thrust force

of the rotor. Equation 3.7 shows this relation, where the reader is referred to [27] for its derivation. Note that the power is dependent on the wind speed with a cubed relation, while the thrust depends on the wind speed quadratically.

Analyzing wakes, using the thrust coefficient C_T makes more sense than using the power coefficient C_p, since the thrust determines the amount of momentum extracted from the wind. Also, when measuring the power (coefficient) many more efficiencies are at play than pure aerodynamics. Looking back at figure B.3 it can be seen that the thrust force is the only force acting on the control volume. Therefore the thrust force is in direct relation with the decrease of wind speed inside the control volume. Interestingly, the maximum efficiency (highest C_P) is not reached at maximum thrust force. From the ideal equation 3.7 if follows that $C_{T_{opt}}(a = \frac{1}{3}) = \frac{8}{9} \approx 0.89$.

It has to be noted that these calculations and the calculations in the rest of the section are performed by only using the momentum theory. In the Master thesis the validity of these calculations need to be thoroughly confirmed. However, it is considered correct enough to prove the point of the mentioned necessity.

The last issue is now that the relation between curtailment and the thrust force is not generally theoretically known. This relation is the last link in the chain to determine the effect of wakes and curtailment on the available power. Turbine manufacturers need to provide this in their documentation.

$$T = \frac{1}{2}\rho V_0^2 A C_T \quad where \quad C_T = 4a(1-a) \tag{3.7}$$

From equation 3.7 it is safe to say that a higher (thrust) loading of the wind turbine, means a higher velocity deficit behind the turbine. Looking at figure B.5 it appears that this is indeed true until $a = \frac{1}{2}$ as after this point u_1 will become negative. It does not mean that the turbine cannot operate after this point, but only that the momentum equation used for the derivation is no longer valid. It therefore needs to be corrected. Figure 3.11 shows two coined corrections [27].

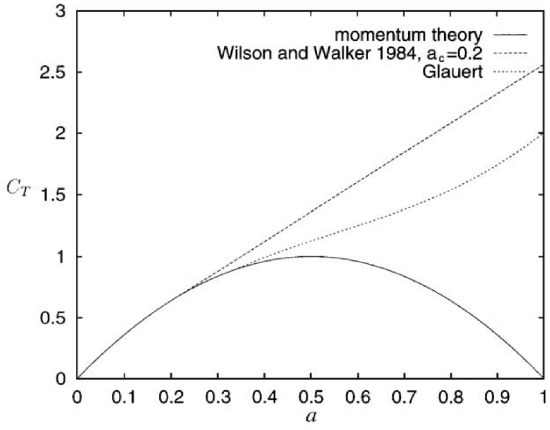

Figure 3.11: Two thrust coefficient corrections for high induction factors [27]

The thrust coefficient depends on the operation parameters of the rotor and the blades. The relevant parameters have implicitly already been defined in section 2.3. Literature showed that the two mechanisms to curtail the power of a wind turbine were either by pitching the blades or overspeeding of the rotor. The impact of overspeeding is analysed using a proxy parameter, namely the tip speed ratio of equation 3.8, where the rotor speed is normalized to the free stream wind velocity. Figure 3.12 shows a possible realization of the dependency of the power coefficient on the pitch angle and the tip speed ratio.

$$\lambda = \frac{\omega R}{V_0} \tag{3.8}$$

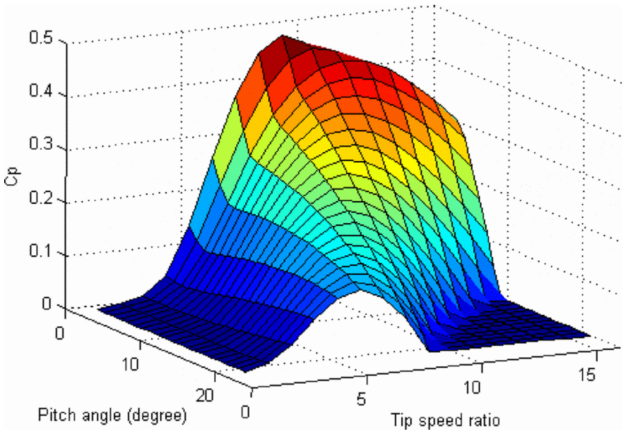

Figure 3.12: A possible realization of the dependency of the power coefficient on the pitch angle and the tip speed ratio [47]

Now that it is clear what determines the value of the thrust coefficient, it is time to look at the effect of the thrust coefficient on the wake. The main characteristics of the wake have been defined as the velocity deficit and the turbulence intensity.

Velocity Deficit

Equation 3.7 shows the relation between the thrust coefficient and the induction factor. This equation can be inverted to equation 3.9, when the insignificant solution for $a > \frac{1}{2}$ is ignored. When the curtailed thrust coefficient is inserted, the curtailed velocity deficit can be obtained.

$$a_c = \frac{1}{2} - \frac{1}{2}\sqrt{1 - C_{T_c}} \tag{3.9}$$

It is of interest to see how a change in thrust coefficient influences the change of the induction factor. This will namely be the actual induction factor created by the turbine and the one that should be used for wake modeling in the next chapter. Using the derivation below, equation 3.11 is obtained. It is noted that this equation is for the ideal

situation. Using the thrust and power curves of the specific turbine, as delivered by the manufacturer, leads to more accurate results. The induction factor during curtailment is implicitly defined using the curtailment factor and the induction factor under normal conditions.

$$\begin{aligned} &C_{P_c} = 4a_c(1-a_c)^2 = C_{T_C}(1-a_c) = (1-\mu)C_P = (1-\mu)C_T(1-a) \\ &\rightarrow C_{T_c} = (1-\mu)\tfrac{1-a}{1-a_c}C_T \end{aligned} \tag{3.10}$$

$$\begin{aligned} a_c &= \tfrac{1}{2} - \tfrac{1}{2}\sqrt{1-C_{T_c}} = \tfrac{1}{2} - \tfrac{1}{2}\sqrt{1-(1-\mu)\tfrac{1-a}{1-a_c}C_T} \\ &= \tfrac{1}{2} - \tfrac{1}{2}\sqrt{1-(1-\mu)\tfrac{1-a}{1-a_c}4a(1-a)} \\ &= \tfrac{1}{2} - \tfrac{1}{2}\sqrt{1-4a(1-\mu)\tfrac{(1-a)^2}{1-a_c}} \end{aligned} \tag{3.11}$$

Figure 3.13 shows the evaluation of equation 3.11 for different operation modes, where r is the ratio between the induction factor during curtailment and under normal conditions. It can be observed that the effect of the curtailment is already considerable for small values of curtailment. At 1% curtailment, the curtailed induction factor has already dropped by 10% with respect to the optimal induction factor $a = \frac{1}{3}$ without curtailment. And for 5% curtailment this value is even 25%. This again, confirms that the effect of curtailment on wakes is very important for the size of the wake. Figure 3.13 shows a strange curve for $a = 0.4$ near $\mu = 0$, which is now contributed to not including corrections, like the Glauert correction.

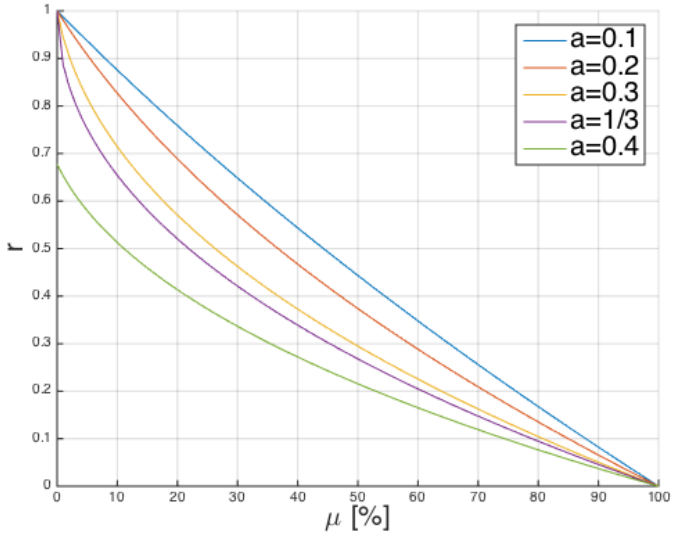

Figure 3.13: The dependency of the velocity deficit on the curtailment for different operating modes. $r = \frac{a_c}{a}$

Turbulence Intensity

As described in section 3.1.3, the added turbulence intensity is depended on the break down of the tip vortices of the blades. Because the magnitude of this vortices depend

on the forces exerted on the control volume, i.e. the thrust force, it is expected that the added turbulence decreases while under curtailment. This is especially important for offshore wind farms, as there the added turbulence is a more significant part of the total turbulence than for onshore wind farms. [48]

3.4. Effect of Wakes on the Available Power Estimators (APE)

Enough calculation and graphs have now been discussed to prove what was mentioned in the introduction of this report: summing all individual APEs does not lead to the AFPE. In order prove this, first the concept of an APE is studied. Then the previous section is used to determine the inequality.

3.4.1. APE

All APEs are in some way based on the power curve as discussed in section B.1. The incoming wind speed is measured at the turbine from which the possible production can be read off the power curve (or theoretically calculated by equation B.1).

The patent of Krishna R. (Siemens Wind Power) [16] describes a method, which is an example of an implementation of such an estimator. The goal of this method is to determine "the estimated wind speed based on the current power, the current rotor speed and the current blade pitch angle", see figure 3.14. For the last step (determining the available power from the estimated wind speed) the methodology of the patent depends on the power curve.

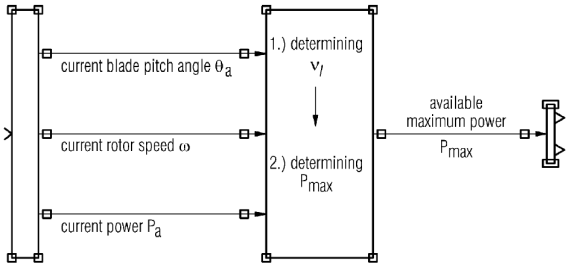

Figure 3.14: A schematic description of the method described by the patent from Krishna R. (Siemens Wind Power) [16] to estimate the available power

The patent describes a method of estimating the wind speed without the usage of the anemometer on top of turbine, as (during curtailment) the wake effects prevent accurate measurements in this manner. As described by section 2.3 the main mechanisms to curtail a wind turbine are overspeeding the rotor and pitching the blades, which is why both signals (rotor speed and blade pitch angle) need to measured. In combination with the measured actual output of the wind turbine the methodology of the patent is able to estimate the available wind power.

The methodology uses equation 3.12, which is comparable to equation B.14, but more generally defined with more dependencies. Parameters T and p are the local temperature and pressure and $\mathcal{V}$ is the wind speed to be determined. The patent also de-

scribes the use of look-up tables and standardization of the parameters R, ρ, p and T to make solving the equation fast and only dependent on the rotor speed, blade pitch angle and actual power generation. As this the thesis is focused on the wake effects on the available power during curtailment and not on the individual power estimation, no further study is performed. The reader is referred to the patent description [16] for more information and patents [49] and [50] for alternative, but very comparable, methods.

$$P_{actual} = C_P\left(\frac{R\omega_{rotor}}{\mathcal{V}(T,p)},\theta\right)\pi\frac{R}{2}\rho(T,p)\mathcal{V}(T,p)^3 \tag{3.12}$$

3.4.2. Example of Two turbines

Consider two indentical turbines, with the wind coming from the same direction as as the line connection the turbines. The power curve of the turbine can be expressed as in equation 3.17. In this example $\frac{1}{2}\rho A = 1000$ and the turbines are operating at optimum efficiency, i.e. $a = \frac{1}{3}$. Let the wind velocity be $10\frac{m}{s}$. The power produced by the first turbine can therefore be calculated as follows.

$$APE_{T1} = P_{T1_{available}} = \frac{1}{2}\rho V_0^3 AC_p = 1000\cdot V_0^3 a(1-a)^2 = 1000\cdot 1000\cdot\frac{4}{27} \approx 148kW \tag{3.13}$$

The power produced by the second turbine is depended on the impact of the wake on the second turbine. A qualitative description has already been provided, but a quantitative description is required in order to calculate its effect in this example. Wake models serve this cause and are discussed in the next chapter. For now, lets assume that 20% of the velocity deficit created by the first turbine is felt by the second turbine. As the induction factor was set to $a = \frac{1}{3}$, the velocity behind the turbine, e.g. u_1 from equation B.11, is equal to $u_1 = (1-2\cdot\frac{1}{3})V_0 = \frac{1}{3}V_0$. Now the incoming wind speed of the second wind turbine can be calculated as $V_{0_{T2}} = \frac{4}{5}V_0 + \frac{1}{5}u_1 = \frac{13}{15}V_0 \approx 0.87V_0$.

The available power of second turbine can therefore be calculated as below. The total available power under uncurtailed conditions is therefore $P_{available} = 244kW$, see equation 3.15.

$$APE_{T2} = P_{T2_{available}} = \frac{1}{2}\rho V_{0_{T2}}^3 AC_p = 1000\cdot\left(\frac{2197}{3375}V_0^3\right)a(1-a)^2 \approx 1000\cdot 651\cdot\frac{4}{27} \approx 96kW \tag{3.14}$$

$$AFPE_{\mu=0} = \sum APE_i = APE_{T1} + APE_{T2} = 148 + 96 = 244kW \tag{3.15}$$

Now let both turbines be curtailed for 10%. The power of the first turbine is easy to calculate as below. However, this leads to operating at a different induction factor. From figure 3.13, it can be seen that for $a = \frac{1}{3}$ and $\mu = 10\%$ the ratio of induction factors is 0.65. The velocity behind the turbine therefore increases to $u_1 = (1-2\cdot 0.65\cdot\frac{1}{3})V_0 \approx 0.56V_0$.

$$APE_{T1_{\mu=10\%}} = P_{T1_{\mu=10\%}} = 0.9P_{T1_{available}} = 0.9\cdot 148 \approx 133kW \tag{3.16}$$

The velocity felt by the second turbine is $V_{0_{T2_{\mu_1=10\%}}} = \frac{4}{5}V_0 + \frac{1}{5}u_1 \approx 0.91V_0$. The available power at the second turbine can now be calculated, using the same calculations of before. It can be seen that the available power for the second turbine rose by 17% to $112kW$.

$$APE_{T2_{\mu=10\%}} = P_{T2_{available_{\mu_1=10\%}}} = 1000 \cdot (0.91 \cdot V_0)^3 \, a(1-a)^2 \approx 1000 \cdot 754 \cdot \frac{4}{27} \approx 112kW \tag{3.17}$$

Now the curtailed power by the second turbine can be calculated as well. The total power by curtailing the two wind turbines each by 10% is $133+101 = 234kW$. This is only a 4% decrease in tot generated power, while both turbines where curtailing 10% of their available power.

$$P_{T2_{\mu=10\%}} = 0.9P_{T2_{available_{\mu_1=10\%}}} = 0.9 \cdot 112 \approx 101kW \tag{3.18}$$

The total available power (i.e. without any curtailment) was $244kW$. When the two available powers of the turbines during curtailment are summed, it results in $260kW$, see equation 3.19. As the wind conditions did not change, the total available power can also not change. Therefore when the the AFPE does not include any wake considerations, it leads to an overestimation of the available wind power during curtailment. In this case this overestimation was 7% for 10% curtailment, noting that only 20% of the velocity deficit created by the wake was felt by the sequential turbine. This is what was stated in the introduction, mathematically shown in equation 3.20 and what will be the topic for the Master thesis.

$$AFPE_{\mu=10\%} = \sum APE_{i_{\mu=10\%}} = APE_{T1} + APE_{T2_{\mu=10\%}} = 148 + 112 = 260kW \tag{3.19}$$

$$AFPE_{\mu} < \sum APE_{\mu_i} \tag{3.20}$$

4

WAKE CALCULATIONS & MODELS

The last chapter finished with an example to demonstrate the effect of wakes on the APE during curtailment. The example focused on the power production of two turbines. The need of a wake model became apparent when the velocity at the second turbine had to be calculated. For the sake of simplicity it was assumed that the wake had been dissipated for 80%. However, the example demonstrated that even this fairly dissipated wake had a big impact in the error of the AFPE.

The purpose of the Master thesis associated with this literature study, is to develop a theoretical and numerical methodology for an AFPE. It is therefore crucial to pay attention to the modeling of the wakes in order to select the best one. Many approaches to this modeling have already been performed, tested and discussed in literature. It is therefore not the goal of the thesis to develop a new model, but merely to select (a combination of) the right one.

The first wake models that are studied fall in the group of engineering models. They approach the wakes as an energy deficit, where only the interesting parameters are calculated from, e.g. the velocity deficit and turbulence intensity at sequential turbines. A second type of wake models come from computational fluid dynamics (CFD). These models approach the wakes from a more fundamental physics perspective. These models are generally more computational expensive, but might result in higher accuracy. After all models have been presented, they will be compared to each other.

Two distinct interests of the wake models can be defined. First, the velocity (or momentum) deficit generated by the wind turbine, which leads to a reduction of available power for the sequential turbines. Second, the increase in turbulence intensity, which has an influence on the dissipation rate of the wake.

4.1. Engineering Wake Models

The wake models in this section are engineering or explicit wake models. They directly calculate the most interesting wake parameter, namely the velocity deficit. They are mostly based on simple equations, corrected and validation by experiments. They have low computational cost and are easy to implement and combine.

The do, however, make a lot of simplifications and assumptions. Some of these assumptions are later compensated for by other articles. These type of models are very interesting for the purpose of the Master thesis, as they are so fast that they enable real-time calculation of the available wind power.

4.1.1. N. O. Jensen

One of the oldest wake models (1983) is often praised by its simplicity. It is a good example of an engineering approach to the complex phenomena of wakes. It only calculates the velocity deficit and the growth of the wake downstream. Notwithstanding its age, it is still widely used, because of its ease of application. This popularity allowed for many validation studies. Most of these studies proved that is still a suitable choice for first order estimates.

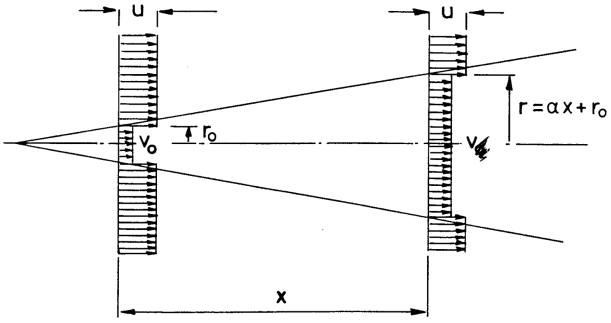

Figure 4.1: Schematic N. O. Jensen single wake model. [51]

The only inputs of the model are the free stream velocity and the wake decay constant. The velocity deficit is considered to happen instantaneous at the position of the turbine. The wake expansion is modeled as linear, see figure 4.1. In equation 4.1 this linearity is defined, with the slope k. Methodologies of determining the right value of this wake decay constant are heavily debated. Choi and Shan proposed to use figure 4.2. It can be seen that for default offshore conditions ($TI = 8\%$) the wake decay factor equals $k = 0.04$.

$$r = kz + R \tag{4.1}$$

Singe Wake Model

Equation 4.2 forms the basis of the Jensen wake model. It is based on the balance of mass (not the conservation of momentum which is mentioned in Jensens original publication [53]).

$$\pi R^2 u_1 + \pi (r^2 - R^2) V_0 = \pi r^2 u(z) \tag{4.2}$$

When equations 4.1 and 4.2 are combined and using the expression of u_1 from equation B.11, an expression for the velocity at downstream distance z is found. In this equa-

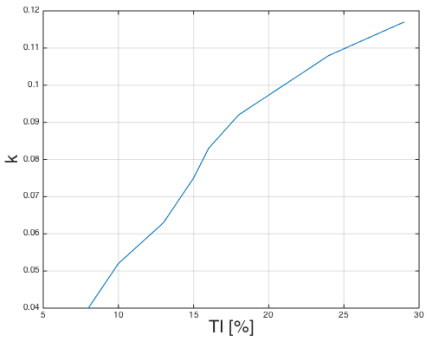

Figure 4.2: Wake decay parameter k dependency on the turbulence intensity. [52]

tion a_1 is the induction factor of the turbine. See figure 4.3 for a visualization of an example of the Jensen model for $V_0 = 10\frac{m}{s}$ and $k = 0.075$.

$$u(z) = V_0\left[1 - 2a_1\left(\frac{R}{R+kz}\right)^2\right] = V_0\left[1 - 2a_1 K(z)^2\right] \quad with \quad K(z) = \frac{R}{R+kz} \tag{4.3}$$

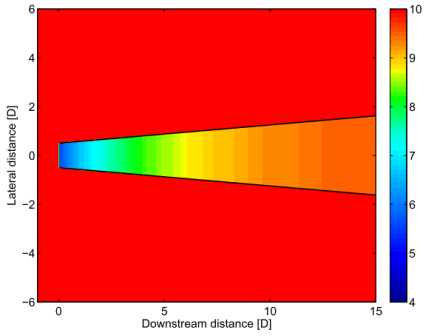

Figure 4.3: An example of the Jensen wake model for $V_0 = 10\frac{m}{s}$ and $k = 0.075$ [46]

Multiple Wake Model

This model can be extended to include multiple sequential wakes. When looking at equation 4.2 the incoming wind speed for the second turbine is not V_0, but $v(z_0)$ where z_0 is the distance between the turbines. Also u_1 needs to be replaced with u_2 as the wind speed behind the second turbine is now important for the mass balance. See figure 4.7 for a qualitative visualization of the multiple wake model. Equation 4.3 can be transformed to calculate the wake after the N^{th} turbine as in equation 4.4. In this equation a_N is the induction factor of the N^{th} turbine and a is the induction factor of each turbine.

$$u_N(z) = V_0\left[1-(1-a_N u_{N-1}(z))\,K(z)^2\right] = V_0\left[1-2aK(z)\frac{1-(aK(z))^N}{1-aK(z)}\right] \tag{4.4}$$

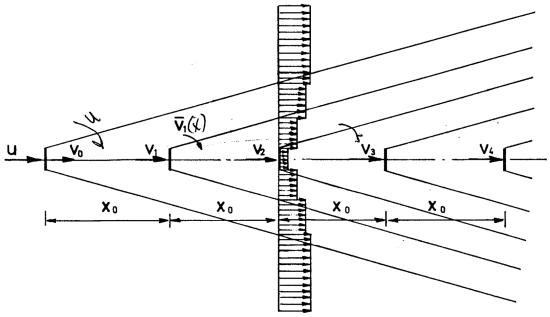

Figure 4.4: Schematic N. O. Jensen multiple wake model [51]

It is important to observe that the Jensen model does not keep reducing the wind speed for multiple wakes, but it reaches an asymptotic value.

$$u_\infty(z) = V_0\left[1-2aK(z)\frac{1-(aK(z))^\infty}{1-aK(z)}\right] = V_0\left[1-2aK(z)\frac{1-0}{1-aK(z)}\right] = V_0\frac{1-3aK(z)}{1-aK(z)} \tag{4.5}$$

Bell Shape Modulation

Both figures 4.1 and 4.7 show that the velocity deficit has a top-hat distribution. r defines the size of the wake at distance z and at these boundaries the velocity suddenly changes. Jensen recognized that this is not similar to the real distribution, which appears to be more bells shaped. He proposed to use the modulation shown in equation 4.6, where θ is the off-axis angle in degrees. See figure 4.5 for the effect of the modulation, where Jensen compared his model to actual wind data. [51]

$$f(\theta) = \frac{1+\cos(9\theta)}{2} \quad with \quad \theta < 20^\circ \tag{4.6}$$

4.1.2. Katic Correction for N. O. Jensen

A noteworthy correction on the Jensen wake model comes from Katic. [54] Katic notes that this correction is interesting for mean energy production analyses and not for additional loads due to increased turbulence. It is therefore considered interesting for the purpose of this report. Katics correction considers the situation where wakes interact.

Katic treats the kinetic energy deficit of these interaction areas as the sum of the energy deficits of the interacting wakes. He therefore finds the energy balance as in equation 4.7

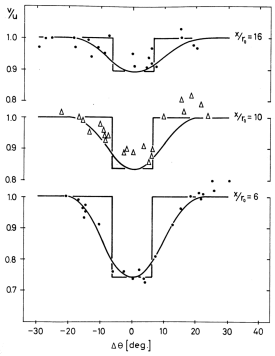

Figure 4.5: Bell shape modulation to simple top-hat model compared to actual wind data [51]

$$\left(1-\frac{u}{V_0}\right)=\left(1-\frac{u_1}{V_0}\right)+\left(1-\frac{u_2}{V_0}\right)+(...)+\left(1-\frac{u_N}{V_0}\right) \tag{4.7}$$

This equation can be generalized to equation 4.8 as it was introduced by [52], where u_i is the wind speed in front of turbine i and $u_{k,i}$ is the wind speed in the wake of turbine k in front of turbine i.

$$u_i = V_0\left[1-\sqrt{\sum_{k=1}^{i-1}\left(1-\frac{u_{k,i}}{V_0}\right)^2}\right] \tag{4.8}$$

4.1.3. Choi and Shan Corrections for N. O. Jensen

As can be observed, the N. O. Jensen wake model, including the Katic correction, is still very simplistic. Although it is a very popular model, several corrections need to be applied to make its results more realistic, accurate and useful for the purpose of the Master thesis. Choi and Shan [52] presented three corrections to include partial wake shadow, yaw misalignment and unsteady wind conditions in the model.

Partial Wake Shadow

Partial wake shadowing refers to a wind turbine that is not fully in the wake of the upstream turbine(s), but on partially. This is very important for the purpose of the Master thesis, as the available wind power needs to be estimated in every wind condition. Choi and Shan calculated than for an equidistant layout of a wind farm with of $7D$ a center turbine is 35% in full a shadow and 29% in a partial shadow, see figure 4.6. However, a wind farm is mostly designed in such a fashion that it have the lowest wake loss depending on the most common wind directions. So these calculations are only valid for an (uncommon) uniform wind direction probability distribution.

In order to account for the partial shadowin, Choi and Shan introduced the shadowing factor β in equation 4.8 from Katic as in equation 4.9. The shadowing factor is defined as the swept area of the turbine that is in the wake normalized to the rotor area of the wake generating turbine.

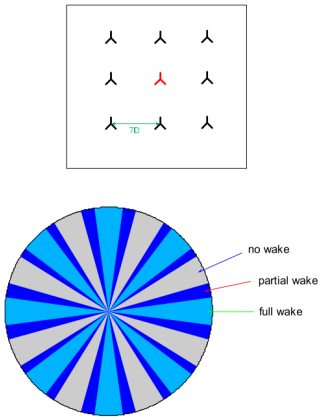

Figure 4.6: Full versus partial wake shadow of a center turbine [52]

$$u_i = V_0 \left[1 - \sqrt{\sum_{k=1}^{i-1} \beta_k \left(1 - \frac{u_{k,i}}{V_0} \right)^2} \right] \tag{4.9}$$

Equation 4.9 is based on the momentum equation, but it is not, however, suitable to calculate the power or thrust force with. As these are integrated with the wind speed cubed and squared respectively, a virtual wind speed need to be defined. The procedure of Choi and Shan is to divide the swept area of the rotor in n sections, which are either in full wake ($\alpha_j = 1$) or not in the wake at all ($\alpha_j = 0$), see equations 4.10 and 4.11. This correction was tested with validation data of the Danish Middelgrunden wind farm and provided a better prediction of the wind speeds than without the correction.

$$u_{i,Power} = \sqrt[3]{\sum_{j=1}^{n} \alpha_j \left(V_0 \left[1 - \sqrt{\sum_{k=1}^{i-1} \beta_k \left(1 - \frac{u_{k,i}}{V_0} \right)^2} \right] \right)^3} \tag{4.10}$$

$$u_{i,Thrust} = \sqrt{\sum_{j=1}^{n} \alpha_j \left(V_0 \left[1 - \sqrt{\sum_{k=1}^{i-1} \beta_k \left(1 - \frac{u_{k,i}}{V_0} \right)^2} \right] \right)^2} \tag{4.11}$$

Yaw Misalignment

As mentioned in section 3.1.6 and 2.3, yawing a wind turbine out of the optimal 90° with the wind decreases the amount of of power the turbine can convert. In order to rightly estimate the available power, this has to be accounted for. Choi and Shan proposed relations for the power and thrust coefficients as in equations 4.12 and 4.13, where C_{P_0} and C_{T_0} refer to the coefficients without yaw.

$$C_P = C_{P_0} \cdot \cos^3(\gamma) \tag{4.12}$$

$$C_T = C_{T_0} \cdot \cos^2(\gamma) \tag{4.13}$$

The maximum power coefficient is now at $a = \frac{\cos(\gamma)}{3}$ (from equation 2.1) instead, but can be defined more generally as in equation 4.14. [52]. Equation 4.3 (and all its derivatives) calculating the velocity in the wake can now be rewritten as in equation 4.15 for yaw.

$$a = \frac{\cos(\gamma) - \sqrt{\cos^2(\gamma) - C_{T_0}\cos^2(\gamma)}}{2} \tag{4.14}$$

$$u(z) = V_0\left[1 - \left(\cos(\gamma) - \sqrt{\cos^2(\gamma) - C_{T_0}\cos^2(\gamma)}\right)K(z)^2\right] \tag{4.15}$$

Unsteady Wind Conditions

Using the Windviewer SDE+ (mentioned in section 2.2.2) from the Dutch government, the wind speed of wind farm Westermeerwind is estimated to have an average of about $8\frac{m}{s}$. As the maximum distance of the wind turbines is $520m$, the time difference between the turbines for the same wind is more than a minute. For bigger offshore wind farms this might even be longer. Since the wind speed and direction are not constant, the wind speed in the wake also changes with time. When modeling the complete wind farm, this delay due to the unsteady wind has to be accounted for.

Equations 4.16, 4.17 and 4.18 are updated versions of equations 4.12, 4.13 and 4.15, respectively.

$$u_{i,Power}(z, t+\Delta t) = \sqrt[3]{\sum_{j=1}^{n}\alpha_j\left(V_0(t)\left[1 - \sqrt{\sum_{k=1}^{i-1}\beta_k\left(1 - \frac{u_{k,i}(z,t+\Delta t)}{V_0(t)}\right)^2}\right]\right)^3} \tag{4.16}$$

$$u_{i,Thrust}(z, t+\Delta t) = \sqrt{\sum_{j=1}^{n}\alpha_j\left(V_0(t)\left[1 - \sqrt{\sum_{k=1}^{i-1}\beta_k\left(1 - \frac{u_{k,i}(z,t+\Delta t)}{V_0(t)}\right)^2}\right]\right)^2} \tag{4.17}$$

$$u(z, t+\Delta t) = V_0(t)\left[1 - \left(\cos(\gamma) - \sqrt{\cos^2(\gamma) - C_{T_0}\cos^2(\gamma)}\right)K(z)^2\right] \tag{4.18}$$

Choi and Shan proposed equation 4.19 to calculate Δt, where it segments the distance between the turbines in n parts.

$$\Delta t = \frac{(n+1)x}{\sum_{i=0}^{n} u(i)} \tag{4.19}$$

4.1.4. Ainslie

Another fairly old model is the Ainslie wake model [55]. It is based on time-averaged Navier-Stokes equations with the concept of Eddy Viscosity (EV) closure. It uses the continuity and momentum equilibria and includes thin shear layer approximation. Most equations are based on experimental wind tunnel data. It can therefore be considered as a hybrid model between an engineering model and a CFD model.

Equation 4.20 forms the basis of this wake model. It calculates the velocity profile at a downstream distance of $2D$ for different radial positions. The parameters D_M and b represent the velocity deficit and the wake width at $2D$, respectively. The distance of $2D$ is chosen by Ainslie as he states that the pressure gradient will no longer dominate the wake at that distance, as can be seen in figure 3.1 due to the Gaussion-like shaped velocity profile.

$$u_{2D} = V_o D_M e^{-3.56(\frac{r}{b})^2} \quad with \quad \begin{aligned} D_M &= C_T - 0.05 - (16C_T - 0.5)\frac{TI}{1000} \\ b &= \sqrt{3.56\frac{C_T}{8D_M(1-0.5D_M)}} \end{aligned} \tag{4.20}$$

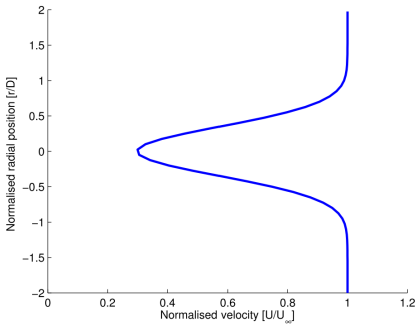

Figure 4.7: Example of Ainslies Gaussian velocity profile at 2D for $C_T = \frac{8}{9}$ and $TI = 10\%$ [53]

In order to calculate the far wake, the momentum and continuity equations are used. Equation 4.21 has combined these equations into a final equation that needs to be solved using the concept of Eddy Viscosity (see [53] for its derivation). The parameter ν_T is referred to as the Eddy Viscosity (EV) term.

$$u\frac{du}{dz} + u_\theta\frac{du}{dr} = \frac{\nu_T}{r}\left(\frac{du}{dr} + r\frac{d^2u}{dr^2}\right) \tag{4.21}$$

Ainslie defined the value of the EV term as in equation 4.22 (rewritten by [53]), where κ is the Von Kármán constant and u_c is the wind speed at the center line. It consists of a term generated by the wind shear in the wake and a term due to the ambient eddy viscosity of the atmospheric flow. The dependency on the downstream distance is defined by the filter function $F(z)$ as in equation 4.23 [55]

$$\nu_T = 0.015F(z)0.5b(V_0 - u_c) + F(z)\frac{TI\kappa}{2.4} \tag{4.22}$$

$$F(\frac{z}{D}) = \begin{cases} \frac{z}{D} < 5.5: & 0.65 + \sqrt[3]{\frac{\frac{z}{D}-4.5}{23.32}} \\ \frac{z}{D} > 5.5: & 1 \end{cases} \tag{4.23}$$

See figure 4.8 for a visualization of an example of the Ainslie wake model. The effect of the filter function is clearly visible. The wake only starts to change after $x/D = 4.5$.

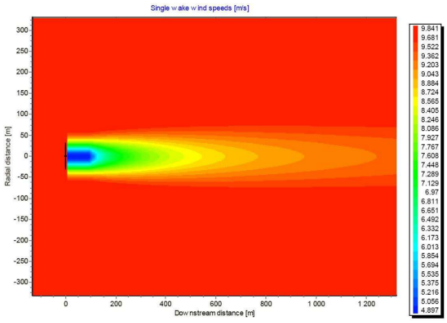

Figure 4.8: An example of the Ainslie wake model [46]

4.1.5. G. C. Larsen

Where Ainslie derived his methodology mostly from empirical data, G. C. Larsen used the streamtube momentum theory and continuity [4]. The Larsen model is a reuse of the Ainslie model and was focused the meandering effect. It is therefore sometimes also referred to as the dynamic wake meandering (DWM) model. As Larsens model was more targeted to be proof of concept, this model has later been improved at lot with respect to accuracy. Van Heemst [53] recommended to use version of Madsen et al. [56] as it is the most elaborate in the discussion on the parameters and contains numerical results, which can be verified.

Larsens expression for the EV-term can be found in equation 4.24, where the constants are calibrated by Madsen [56]. The filter functions F_1 and F_2 are different than from Ainslie, see figure 4.9.

$$\nu_T = 0.008 F_2 \frac{0.5b}{R}\left(1 - \frac{u_c}{V_0}\right) + 0.07 F_1 TI \tag{4.24}$$

4.1.6. S. Frandsen

The Storpark Analytical Model (SAM) or Frandsens model is a new model from 2006 developped by Frandsen et al. [44] It was created to provide a good model for larger (offshore) wind farms by including both small and large scale flow features. It consists of three defined regimes as in figure 4.10. The first regime consists of multiple wakes of sequential (single row) turbines. The second regime is where lateral wakes interfere which each other and merge. The third regime starts where the wakes are in balance with the

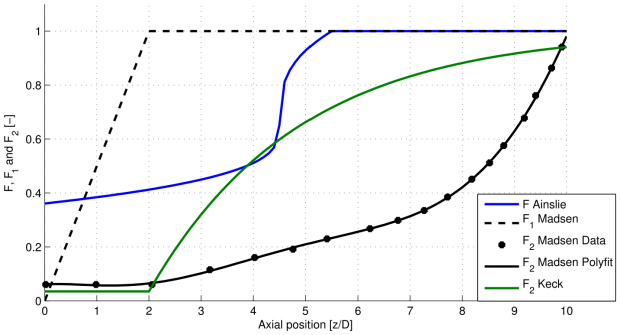

Figure 4.9: Filter functions for Ainslie [55] and Larsen [4] (as by Madsen [56]) wake models [53]

4

atmosphere, e.g. the wake does not become severe nor does it diffuse. The model is a combination of analytical and empirical parts.

The Frandsen model seems to be a very interesting model for the application of available power estimation as it is consists of several modules. The definition of the three different regimes, allow validation of the AFPE model for each of these regimes. For the Master thesis it can be looked into if this regime-based system can be used in combination with other wake models.

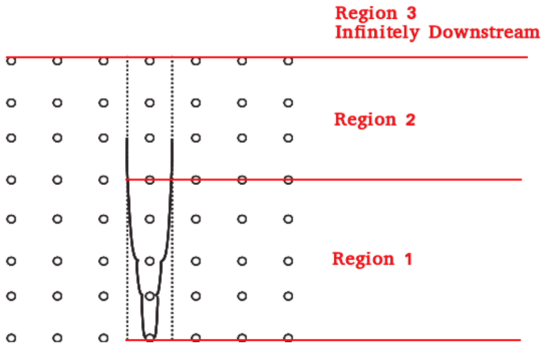

Figure 4.10: The three regimes of the Frandsen model [53] [44]

First Regime

The main equation of the first regime (multiple wake, single row) of the Frandsen model is defined in equation 4.25. It defines the wake expansion with a simple top-hat profile. Self-similarity is assumed in this region, as the article of the model is mostly interested in large wind farms. The value of α needs to be defined empirically.

$$D(z) = \left(\beta^{\frac{3}{2}} + \alpha\frac{z}{D_0}\right)^{\frac{1}{3}} D_0 \quad with \quad \beta = \frac{1+\sqrt{1-C_T}}{2\sqrt{1-C_T}} \tag{4.25}$$

Using the momentum equation the velocity deficit can be defined as in equation 4.26. See Frandsen et al [44] for its full derivation.

$$u = V_0\left(1 - a\frac{A_0}{A}\right) \tag{4.26}$$

This equation can be used to find the wake deficit of the N^{th} turbine, using the recursive equation 4.27. It is important to use the right value of the area, meaning that the area occupied by the ground should be excluded (i.e. the model violates the self-similarity assumption).

$$u_{n+1} = V_0\left[1 - \left(\frac{A_n}{A_{n+1}}(1 - \frac{u_n}{V_0}) + \frac{A_R}{A_{n+1}}\frac{C_T u_n}{2V_0}\right)\right] \tag{4.27}$$

Just as for the Jensen model, the Frandsen model reaches a assymptotic value after a few turbines. In figure 4.11 this attymptotic value can be seen after the fourth turbine.

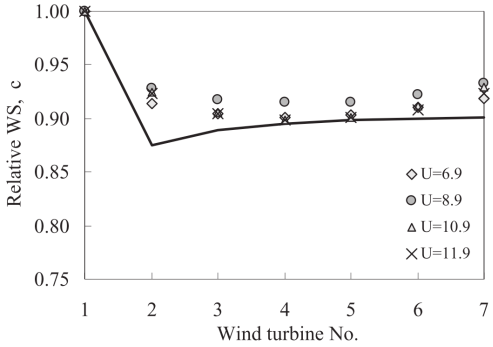

Figure 4.11: Measurements of the wind speed ratio $c = \frac{u}{V_0}$ at Norrekaer Enge II wind farm and the Frandsen model (line). [44]

Second Regime

The second regime (the merging of neighboring wakes) uses the output of the first regime as the initial conditions. The height of the wake is calculated as in equation 4.28, where z_0 and h_0 are taken from regime 1. The parameter s_r and s_f are the non-dimensional distances between neighboring turbines.

$$h = \frac{c_{mw}}{1 - c_{mw}} c_t(z - z_0) + h_0 \quad with \quad c_t = \frac{\pi C_T}{8 s_r s_f} \tag{4.28}$$

Frandsen uses figure 4.12 to support equation 4.28. Although his model does not correspond well with the Elliott model, he refers to literature that recommends a correction value for the Elliott model of 0.33, based on experimental evidence. With this correction factor his model seems to fit well.

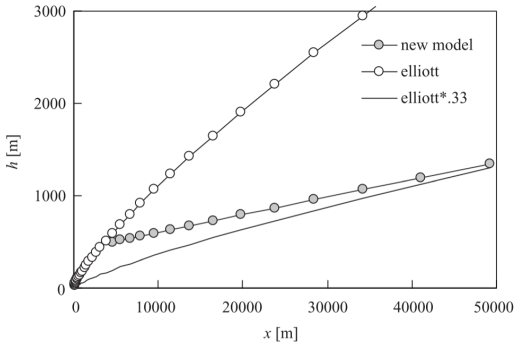

Figure 4.12: Growth of wake in second regime [44]

Third Regime

In his original publication Frandsen et al. did not extensively treat the third regime. Rathmann et al. [57] however did. He used a geostrophic drag-law, see equation 4.29. It is used in order to calculate the wind speed at height h with equation 4.30. The geostrophic drag is dependend on the Coriolos parameter f and the modified geostrophic drag-law constsant $A_* \approx 4$. The parameter z_0 is the surface roughnouss parameter.

$$G \approx \frac{\mu_*}{\kappa}\left(\ln\left(\frac{G}{f z_0}\right) - A_*\right) \tag{4.29}$$

In equation 4.30 the parameter i is a type of turbulence intensity. For the complete implementation of this algorithm, the reader is referred to [57].

$$u(h) = \frac{G}{1 + \left(\ln\frac{G}{hf} - A_*\right) i} \tag{4.30}$$

4.2. CFD Wake Models

The previous treated engineering models can be considered to be more of a phenomenological approach of the complexity of wake flow. This section will treat several models based on computational fluid dynamics (CFD) that try to solve the fundamental physics-based Navier-Stokes equations. Although CFD is very useful for analyzing laminar steady flows, for unsteady turbulent it becomes much more complex quickly.

4.2.1. Navier-Stokes Equations

The Navier-Stokes equations are considered to be able to calculate the exact behavior of a fluid in unsteady, compressible, three-dimensional viscous flow (provided that all the boundary and initial conditions are known) as they include all relevant parameter of a flow: velocity, pressure, temperature and density. They are based on the Euler equations and consist of a time-dependent continuity equation (4.31), three time-dependent conservation of momentum equations (4.32, 4.33, 4.34) and a time-dependent conservation of energy equation (4.35) as can be seen below.

The four independent parameters are the spacial positions x, y and z and the time t. Six dependent parameters can be observed: pressure p, density ρ, temperature T and the three velocity components u, v and w, respectively. The parameters λ and μ are viscosity coefficients for laminar flow with ϵ to account for the turbulent (eddy) part. Parameters q and k are the heat and the heat coefficient, with κ to account for the eddy conductivity. The exact definition or expression of these parameters remain a state-of-the-art research question after 80 years of their implementation.

For the derivation of these equations the reader is referred to the in-depth explanation of [58], they are merely stated here to show their complexity and, above all, their magnificence.

$$\frac{\delta\rho}{\delta t} + \frac{\delta(\rho u)}{\delta x} + \frac{\delta(\rho v)}{\delta y} + \frac{\delta(\rho w)}{\delta z} \tag{4.31}$$

$$\rho\frac{\partial u}{\partial t} + \rho u\frac{\partial u}{\partial x} + \rho v\frac{\partial u}{\partial y} + \rho w\frac{\partial u}{\partial z} = -\frac{\partial p}{\partial x} + \frac{\partial}{\partial x}\left(\lambda\nabla\cdot\vec{V} + 2\mu\frac{\partial u}{\partial x}\right) + \frac{\partial}{\partial y}\left[\mu\left(\frac{\partial v}{\partial x} + \frac{\partial u}{\partial y}\right)\right] + \frac{\partial}{\partial z}\left[\mu\left(\frac{\partial u}{\partial z} + \frac{\partial w}{\partial x}\right)\right] \tag{4.32}$$

$$\rho\frac{\partial v}{\partial t} + \rho u\frac{\partial v}{\partial x} + \rho v\frac{\partial v}{\partial y} + \rho w\frac{\partial v}{\partial z} = -\frac{\partial p}{\partial y} + \frac{\partial}{\partial x}\left[(\mu+\epsilon)\left(\frac{\partial v}{\partial x} + \frac{\partial u}{\partial y}\right)\right] + \frac{\partial}{\partial y}\left(\lambda\nabla\cdot\vec{V} + 2(\mu+\epsilon)\frac{\partial u}{\partial y}\right) + \frac{\partial}{\partial z}\left[(\mu+\epsilon)\left(\frac{\partial w}{\partial y} + \frac{\partial v}{\partial z}\right)\right] \tag{4.33}$$

$$\rho\frac{\partial w}{\partial t} + \rho u\frac{\partial w}{\partial x} + \rho v\frac{\partial w}{\partial y} + \rho w\frac{\partial w}{\partial z} = -\frac{\partial p}{\partial z} + \frac{\partial}{\partial x}\left[(\mu+\epsilon)\left(\frac{\partial u}{\partial z} + \frac{\partial w}{\partial x}\right)\right] + \frac{\partial}{\partial y}\left[(\mu_\epsilon)\left(\frac{\partial w}{\partial y} + \frac{\partial v}{\partial z}\right)\right] + \frac{\partial}{\partial z}\left(\lambda\nabla\cdot\vec{V} + 2(\mu+\epsilon)\frac{\partial w}{\partial z}\right) \tag{4.34}$$

$$\begin{aligned}\rho\frac{D}{Dt}\left(e + \frac{V^2}{2}\right) &= \rho\dot{q} + \frac{\partial}{\partial x}\left((k+\kappa)\frac{\partial T}{\partial x}\right) + \frac{\partial}{\partial y}\left((k+\kappa)\frac{\partial T}{\partial y}\right) + \frac{\partial}{\partial z}\left((k+\kappa)\frac{\partial T}{\partial z}\right) - \nabla\cdot p\vec{V} \\ &+ \frac{\partial(u\tau_x x)}{\partial x} + \frac{\partial(u\tau_y x)}{\partial y} + \frac{\partial(u\tau_z x)}{\partial z} \\ &+ \frac{\partial(v\tau_x y)}{\partial x} + \frac{\partial(v\tau_y y)}{\partial y} + \frac{\partial(v\tau_z y)}{\partial z} \\ &+ \frac{\partial(w\tau_x z)}{\partial x} + \frac{\partial(w\tau_y z)}{\partial y} + \frac{\partial(w\tau_z z)}{\partial z}\end{aligned} \tag{4.35}$$

The goal of CFD programs is to solve these equations to the best of their effort. Solving these equations exactly is practically nearly impossible for wind turbines as the Reynolds numbers are too high, i.e. in the order of $\mathcal{O}(10^6)$. In order to keep the computational effort within bounds, many simplifications and assumptions have been tried and tested. These simplifications are referred to as closure models. The following sections will describe such methods.

4.2.2. Reynolds Averaged Navier-Stokes (RANS)

In the Reynolds Averaged Navier-Stokes (RANS) method, the turbulent fluctuations are averaged. Also, in many cases the flow is assumed to be steady. However, there are some sources of unsteady flow with respect to wind turbine flows: the rotation of the blades, the turbulence of the inflow, the stall of turbine blades, deflection of the blades and the tower shadow. [33] With regard to this literature study, only the first two sources are expected to have a significant influence on the wake.

A second assumption is that the flow of wind turbines can be considered incompressible, as the tip speed generally never exceeds 100 $\frac{m}{s}$. [28] [33] This reduces the complexity of the Navier-Stokes equations greatly.

A disadvantage of RANS is that it is unable to solve for flow separation. As was discussed in section 2.3, pitching the blades to curtail wind power is a common practice.

During this pitching, stall occurs on the blade. Therefore a stand alone RANS simulation seems inappropriate for wind turbine flow analysis. The Detached Eddy Simulation of section 4.2.3 will elaborate on a hybrid method.

4.2.3. Large Eddy Simulation (LES)

Large Eddy Simulation (LES) saves computational effort by filtering out small scale eddies. Only large eddies are calculated, while for the smaller eddies a scale model is used. The assumption is made that these smaller eddies have a universal character and do not depend on the geometry of the flow. LES is more computational expensive than the RANS models, but the accuracy is also increased significantly as the flow is treated as unsteady (at least for scales larger than the grid size).

Generally, using LES the forces acting on the fluid are calculated directly from the solid boundaries of the object, i.e. the blades for wind turbines. This is however exactly what poses a problem for large eddy simulations. Near the object (or near walls) there are few opportunities for filtering smaller eddies as these are the governing scale of interest. Using LES for the complete domain is therefore not advised for wind turbine wake analysis.

Detached Eddy Simulation (DES)

Detached Eddy Simulation (DES) is a combination of LES and RANS. As was mentioned in section 4.2.2 RANS is unable to solve for flow separation. Also, LES becomes very computational expensive in the vicinity of walls. [33] The idea of DES is to combine fine-tuned RANS technology in the boundary layers with the simple power of LES in the separated regions. In the RANS region the turbulence model has full control over the solution through eddy-viscosity based closure, as the Ainslie wake model. In the LES region the larger eddies are resolved and grid refinement can expand the range of scales in the solution. [28] The reader is referred to [59] to see an example of an DES study on the NREL Phase-VI wind turbine blades. Although this models seems promising, it seems to be too complex and too much focused on the blade aerodynamics to be useful for wake analysis.

Actuator Disc/Line - LES (AD/L-LES)

In the aforementioned blind test [60] one of the methods to analyze the wake was a combined actuator disc or line and LES method. In this method the forces on the flow as generated by the rotor are not calculated from the blade boundaries directly, but represented by (a) rotating actuator disc/lines instead. The rest of the domain is solved, using the Navier-Stokes equations on a fine mesh. Just as with normal LES, the sub-grid turbulence is modeled. The large scale turbuelence is predicted directly from Navier-Stokes.

An advantage of this method is that the accuracy is very comparable to normal LES, but the computational effort is much lower. This statement is made based on the assumption that the input from the actuator disc/line is accurate as this generally forms the bottleneck of this method. When this is merely based on a simple BEM implementation the accuracy of this method risk to fall short.

From the blind test and another more primitive version of the AD-LES[61], it is found that this method provides accurate results. It is therefore concluded that from all CFD

Table 4.1: Comparison of discussed engineering wake models

	Assumptions		Support				
Wake Model	Axis-symmetry	Far wake	Wake interference	Yaw misalignment	Added turbulence included	Wake meandering	Low computational effort
N. O. Jensen	Y	Y	N	N	N	N	Y
Improved N. O. Jensen	N	Y	Y	Y	N	N	Y
G. C. Larsen (DWM)	Y	Y (2D)	N	N	Y	Y	M
S. Frandsen	Y	Y (2D)	Y	N	N	N	Y

methods, the AD/L-LES method seems to be the most promising for the application of wake analysis for available power estimation during curtailment with respect to computational expense and accuracy.

4.2.4. A Concluding Remark on CFD

After the literature study, it was concluded that CFD analysis is computationally too expensive with respect tot the accuracy it provides with respect to turbulence, see section 5.2. Also, when performing such accurate calculations, the initial conditions of the calculation have to be defined very accurately as well. For large (offshore) wind farms this is considered unfeasible. However, it is still interesting to present some main research streams, as it can provide knowledge to implement the engineering models better. Also, it might be interesting to look into the possibility to use CFD once to analyze the wind farm in order to generate look-up tables for further wake analysis during curtailment.

4.3. Comparison Wake Models

Table 4.1 shows a comparison of the engineering wake models treated in section 4.1. The CFD wake models are omitted as they are considered of less importance for the cause of the Master thesis. It is considered a task of the Master thesis to make a final decision on the right wake model.

In table 4.1 with the improved N. O. Jensen wake model both the corrections of Choi and Shan [52] and Katic et al. [54] are included. As Larsens model is considered as a reuse of the Ainslie model, the Ainslie model itself is omitted in this comparison.

4.4. A Note on Software Packages

In most of the referenced articles on wake models, the analyses are not performed by manually programming the wake model into a code like MATLAB or Python. Software tools, like windPRO (from EMD International A/S), WindSim (from WindSim AS), WindFarm (from ReSoft Ltd) or WindFarmer (from DNV-GL), are able to do this for different sets of wake models. As the associated company Ventolines BV uses windPRO for its simulations, modeling will start in (but not stay limited to) this software package. However, WindSim also made their software available for this project. So a comparison between these software packages for the purpose of wake modeling during curtailment will be presented in the Master thesis report.

5

Delineation of Scope & Outline Master Thesis

This literature study encompasses many theories, phenomena and approaches that add to the understanding of the effect of wakes on the available power during curtailment. Although some sections were already able to conclude that it did not apply (enough) to get this understanding, this chapter will provide the full delineation of the scope of the Master thesis. First, the problem statement is defined in detail, using all chapters of this report. Second, the scope of the Master thesis to solve this problem is delineated with the findings of the literature. Finally, a general outline of the Master thesis is presented.

5.1. Problem Statement

In chapter 3 it was proved that summing the estimations of the available power from all individual turbines, is not a correct approach to find the total available power of the wind farm during curtailment. The reason is that the decrease in wakes between turbines due to the curtailment, increase the wind speed for the downstream turbines. These downstream turbines estimate their available wind power therefore too high and they cannot achieve this power production, when the upstream wind turbine stops its curtailment.

Chapter 2 showed that there are several reasons for wind farms to curtail their production. TSOs need a good estimation of the available wind power of a wind farm in order to calculate their power reserves. Also, during forced curtailment, an accurate calculation of the production loss is required to determine the right compensation.

Chapter 4 showed that these wake effects are rather complex and the modeling of it is much debated. Therefore, a need arises for an integrated model that can accurately determine the available wind power during curtailment taking these effects into account. The problem statement for the Master thesis can therefore be formalized as:

There is no reliable, fast and accurate methodology to calculate the available wind power of wind farms, when they are under curtailment as the wake effects are not included yet.

5.2. Delineation of Scope

With this clear definition of the problem of the previous section, this section will determine what will be included in the methodology and what it will be targeted to, taking into account this literature study.

5.2.1. Target Wind Farms

The purpose of the Master thesis is to develop an theoretical and associated numerically methodology to determine the available wind power of a wind farm. As the main necessity of this methodology is the effect of wakes during curtailment, it will only be targeted to wind turbines that are clustered into a wind farm and where turbines are placed into each others far wakes.

At this time there seems to be no need to require that these turbines need to be of the same type. However, it is expected that this will reduce the complexity of the methodology, so in the Master thesis this might be decided otherwise. It is required that the turbines are able to provide power control using pitching and overspeeding as defined in section 2.3.

The wake effects that are taken into account are only those that result from previous wind turbines in the wind farm. Therefore, the methodology is only targeted to wind farms that do not have complex environments like mountains and high buildings. This requires different a wake analysis that is not treated in this literature study.

5.2.2. Approach to Wake Modeling

Several wake models are proposed in this report. It is the task of the Master thesis to find the appropriate or a combination of appropriate wake models for the methodology. A trade-off has to be made between low computational time, that allows real-time analysis of the available wind power, and accuracy. CFD analysis might prove to be useful to generate look-up tables of the wind farm to increase the accuracy of engineering models. Using CFD models for the real-time estimation of the available wind power seems unfeasible at this time. The most promosing wake models found are the improved N. O. Jensen wake model and the S. Frandsen wake model.

Wake details as wake meandering, yawed flow, the wake shear layer, vorticity, and axial assymmetry are taken into account as much as possible if this will proof to increase the accuracy for the power estimation. The most important aspect of the wake modeling for the purpose of the Master thesis is to make it as fast and reliable as possible. It might be found that omitting certain wake effects that are treated in this study will have a beneficial effect on the produced methodology. This will be showed by a sensitivity analysis.

5.2.3. Power Estimation

As modern turbines are able to provide data about their individual power estimation, it will be looked into to use this data in the methodology. This will increase reliability of the methodology with respect to estimating the available wind power independently. It is assumed that the signals from the individual turbine power estimators and the provided power curves of the turbines are correct within a defined bandwidth.

5.2.4. Approach Methodology

As many wind farm designers make use of commercially available software, like windPRO and WindSim, the goal of the Master thesis is to deliver a tool that can be used with these software packages. However, where deemed required independently programmed software in MATLAB will be used, while backing up everything with the appropriate theoretical background. The methodology will be tested against the wind farm Westermeerwind. If other validation options are available as well, these will also be looked into.

5.3. Outline Master Thesis

This last section of the literature study provides a general outline of the Master thesis, describing the tasks in more detail and elaborating on the deadline and associated supervisors.

5.3.1. Subdivision Tasks

Before the modeling of wind turbines under curtailment can be performed, first a modeling of a normal operating wind farm needs to be created.

Second, this methodology has to be altered to include the defined effects of wakes in a wind farm during curtailment. It has to be determined which effects are important in which cases how the methodology can make this decision. Using the data provided from the individual available power estimators, the actual available power on farm level needs to be calculated.

Third, this methodology needs to be made available in the mentioned software packages.

Fourth, this methodology will be validated against validation data from Westermeerwind and/or other wind farms. Discrepancies resulting from this validation need to be explained and the methodology must be adapted to account for these discrepancies.

Fifth, a sensitivity analysis will be performed to investigate the effect of the input parameters on the methodology. These can for example be the farm layout, the turbine characteristics and the effect of atmospheric turbulence.

5.3.2. Deadline

As the amount of ECTS points (European Credit Transfer and Accumulation System) for the Master thesis is set on 30, the expected duration is six months. Therefore, the expected date of handing in the Master thesis is set to the end of July, with the note that this will continuously be reviewed.

5.3.3. Supervisors

The thesis is part of the European Wind Energy Master (EWEM), which is a collaboration between four universities in Europe. In case of successful graduation, degrees will be awarded by both the Delft University of Technology as the Norwegian Institute of Science and Technology. Therefore, supervisors from both universities are part of this thesis.

With the supervisors from NTNU, e.g. professor Lars Sætran and Jan Bartl, it was agreed that the main responsibility of supervising would be at the end of the TU Delft. However, they are both available for consultation and guidance and will help with all

necessary formalities required for obtaining the degree from NTNU.

From the associated company Ventolines BV, ir Ardaan Walvis will act as company supervisor, while dr ir Bart Ummels will be available as consultant.

Finally, ir Sebastian Sanchez will be the *daily* supervisor from the TU Delft under supervision of professor dr ir Michiel Zaayer and will help with all neccesary formalities required for obtaining the degree from the TU Delft. Biweekly meetings be organized to assure achieving the tasks of the Master thesis.

NOMENCLATURE

List of Abbreviations

AFPE	Available Farm Power Estimator
APE	Available Power Estimator
TSO	Transmission System Operator

List of Symbols

A	(Swept rotor) area	$[m^2]$
A_1	Wake area in far wake	$[m^2]$
a	(Axial) induction factor	$[-]$
a'	Tangential induction factor	$[-]$
B	Number of blades	$[-]$
C_P	Power coefficient	$[-]$
C_n	Normal force coefficient	$[-]$
C_T	Thrust coefficient	$[-]$
C_t	Tangential force coefficient	$[-]$
c	Airfoil chord length	$[m]$
D	Rotor diameter	$[m]$
F	Force	$[N]$
f	Force per mass per second	$[\frac{N}{kg \cdot s}]$
h	Height of wake	$[m]$
k	Wake decay factor	$[-]$
m	Shear component	$[-]$
$\dot{m}$	Mass flow	$[\frac{kg}{s}]$
P	(Rated) power	$[W]$
p	Pressure	$[Pa]$
p_0	Atmospheric pressure	$[Pa]$
R	Rotor radius	$[m]$
r	Radial position	$[m]$
T	Thrust force	$[N]$
TI	Turbulence intensity	$[-]$
u	Wind speed at rotor	$[\frac{m}{s}]$
u_1	Wind speed in far wake	$[\frac{m}{s}]$
u_i	Wind speed after i^{th} turbine	$[\frac{m}{s}]$
V_0	Free-stream wind speed	$[\frac{m}{s}]$
z	Elevation	$[m]$

α	Angle of attack	$[°]$
β	Shadowing factor	$[-]$
Γ	Vorticity strength	$[Hz]$
γ	Flow yaw angle	$[°]$
κ	Von Kármán constant	$[-]$
ν_T	Eddy viscosity term	$[-]$
ϕ	Flow angle	$[°]$
ρ	Air density	$[\frac{kg}{m^3}]$
σ	Annular area	$[m^2]$
σ_u	Standard deviation wind speed	$[\frac{m}{s}]$
θ	Twist angle	$[°]$
λ	Tip speed ratio	$[-]$
μ	Curtailment factor	$[-]$
μ_u	Mean wind speed	$[\frac{m}{s}]$
ω	(Rotor) rotational speed	$[\frac{rad}{s}]$
χ	Skew angle	$[°]$

List of Figures

2.1 Power curve of a overplanted wind farm, showing the beneficial overplanted power and the lost curtailed power. The x-axis denotes the wind speed in $[\frac{m}{s}]$ [9] . . . 7
2.2 Primary, secondary and tertiary frequency control reserves [15] . . . 8
2.3 Stabilizing capacity of a wind farm without curtailment. [15] . . . 9
2.4 Stabilizing capacity of a wind farm being curtailed for 5% curtailment. [15] 9
2.5 Settled imbalance of Dutch TSO TenneT. The red crosses indicate settlements with a price higher than €50 $\frac{€}{MWh}$ [17] . . . 10
2.6 Settled prices for imbalance of Dutch TSO TenneT. The X-axis shows the time since December 19^{th}, 2015 at 00:00 in program time units (PTU) in 15 minutes for one week. [20] . . . 11
2.7 Increase in market growth of interesting part of power curtailment market for wind turbines (compensation higher than 50 $\frac{€}{MWh}$), see table 2.1 [17][20] 13
2.8 Curtailment mechanisms B pitching (pitch angle β) and C overspeeding ($\Delta\omega_r$) compared to default operation A [11] . . . 14
2.9 Required pitch angles for different amount of curtailments (delta P) depending on the wind speed. [22] . . . 15
2.10 Required rotor speeds for different amount of curtailments (delta P) depending on the wind speed. [22] . . . 16
2.11 Required yaw angles for different amount of curtailments depending on the induction factor. [22] . . . 16

3.1 Alternation of near and far wakes behind five consecutive turbines [30] . . 18
3.2 The shear layer of the actuator disk as a result of the vorticity in the wake [32] . . . 19
3.3 Shear layer developing with distance [33] . . . 20
3.4 Effect of turbulence intensity, shear and stratification on the vortex decay of a single vortex (SV) and a vortex pair (VP) as a function of the non-dimensional time[35] . . . 21
3.5 A visualization of added turbulence [4] . . . 21
3.6 Added turbulence due to neighboring turbines standing at 0° and 180° for the Middelgrunden wind farm. The values I_{pw} are from measurements, while the values of the WAT model are for a model discussed in the article.[37] 22
3.7 Wake visualization of sheared flow. [38] . . . 23
3.8 Influence hub height and thrust coefficient on the vertical shift of the in ground effect. The left graph is for a thrust coefficient of 0.64, while the right graph is for a thrust coefficident of 0.89. [38] . . . 23
3.9 Visualizations of wake meandering [4] . . . 24

3.10 Wake angle due to yawed incoming flow [33] . . . 25
3.11 Two thrust coefficient corrections for high induction factors [27] . . . 27
3.12 A possible realization of the dependency of the power coefficient on the pitch angle and the tip speed ratio [47] . . . 28
3.13 The dependency of the velocity deficit on the curtailment for different operating modes. $r = \frac{a_c}{a}$ . . . 29
3.14 A schematic description of the method described by the patent from Krishna R. (Siemens Wind Power) [16] to estimate the available power . . . 30

4.1 Schematic N. O. Jensen single wake model. [51] . . . 34
4.2 Wake decay parameter k dependency on the turbulence intensity. [52] . . . 35
4.3 An example of the Jensen wake model for $V_0 = 10\frac{m}{s}$ and $k = 0.075$ [46] . . . 35
4.4 Schematic N. O. Jensen multiple wake model [51] . . . 36
4.5 Bell shape modulation to simple top-hat model compared to actual wind data [51] . . . 37
4.6 Full versus partial wake shadow of a center turbine [52] . . . 38
4.7 Example of Ainslies Gaussian velocity profile at 2D for $C_T = \frac{8}{9}$ and $TI = 10\%$ [53] . . . 40
4.8 An example of the Ainslie wake model [46] . . . 41
4.9 Filter functions for Ainslie [55] and Larsen [4] (as by Madsen [56]) wake models [53] . . . 42
4.10 The three regimes of the Frandsen model [53] [44] . . . 42
4.11 Measurements of the wind speed ratio $c = \frac{u}{V_0}$ at Norrekaer Enge II wind farm and the Frandsen model (line). [44] . . . 43
4.12 Growth of wake in second regime [44] . . . 44

A.1 Wind farm cluster *Windpark Noordoostpolder*. The green marked wind turbines are part of the wind farm Westermeerwind related to this report[62] 67

B.1 Power Curve for the NTK 500/41 wind turbine for both stall and pitch control [27] . . . 70
B.2 Effect of pitch angle on the power curve. Positive pitch angle lead to feathered conditions, while negative pitch angles cause blade stall. [23] . . . 71
B.3 Expansion of the streamlines with out of plane circular area $A = \pi R_{rotor}^2$ [27] 72
B.4 Pressure and velocity upstream and downstream of the rotor [27] . . . 72
B.5 The power and thrust coefficient against the induction factor (equation B.15) [27] . . . 75
B.6 Glauerts optimum power coefficient with respect to the Betz limit ($\frac{16}{27}$) against the tip speed ratio. . . . 75
B.7 Angles, velocities and induction factor for the BEM method [63] . . . 77
B.8 Elementary Vortex Flow [58] . . . 78
B.9 Flow Separation [58] . . . 78
B.10 Wing tip vortex of finite wing (airplane) [64] . . . 78

List of Tables

2.1 Overview of market size power curtailment for last few years [17][20] . . . 12

4.1 Comparison of discussed engineering wake models 47

REFERENCES

[1] T. Ackermann, *Energy Sources*, Tech. Rep. (Regeringskansliet, 2008).

[2] T. G. Bozkurt, G. Giebel, N. K. Poulsen, and M. Mirzaei, *Wind Speed Estimation and Parametrization of Wake Models for Downregulated Offshore Wind Farms within the scope of PossPOW Project,* Journal of Physics: Conference Series **524**, 012156 (2014).

[3] M. Vestas, *V164-8.0 MW® breaks world record for wind energy production,* (2014).

[4] G. C. Larsen, *Dynamic wake meandering modeling*, Vol. 1607 (Risø National Library, 2007).

[5] G. Koustas, G. Papaefthymiou, M. Ieee, and B. C. Ummels, *Stochastic Assessment of Opportunities for Wind Power Curtailment,* Power , 1 (2007).

[6] M. R. Skjelmose, *Down-regulation Practices , Available Power Estimation and PossPOW experience,* PossPOW workshop (2015).

[7] Energinet.dk, *Kompensation til havvindmølleparker ved påbudt nedregulering*, Tech. Rep. december 2015 (Energinet.dk, 2014).

[8] C. Warmer, M. Hommelberg, I. Kamphuis, Z. Derzsi, and J. Kok, *Wind Turbines and Heat Pumps - Balancing wind power fluctuations using flexible demand,* 6th International Workshop on Large-Scale Integration of Wind Power and Transmission Networks for Offshore Wind Farms , 1 (2006).

[9] T. Tennet, *POSITION PAPER Overplanting*, Tech. Rep. (TenneT, 2015).

[10] N. P. Spot, *The Power Market,* (2016).

[11] F. Díaz-González, M. Hau, A. Sumper, and O. Gomis-Bellmunt, *Participation of wind power plants in system frequency control: Review of grid code requirements and control methods,* Renewable and Sustainable Energy Reviews **34**, 551 (2014).

[12] P. Tielens and D. van Hertem, *Grid Inertia and Frequency Control in Power Systems with High Penetration of Renewables,* Status: Published , 1 (2012).

[13] M. Milligan, P. Donohoo, and D. Lew, *Operating Reserves and Wind Power Integration: An International Comparison,* 9th Annual International Workshop on Large-Scale Integration of Wind Power into Power Systems , 1 (2010).

[14] UCTE, *Glossary Operation Handbook Entso-e,* Memory **15**, 1 (2004).

[15] J. N. Sakamuri, *Importance of Down-Regulation of WPPs for Power System Ancillary Services,* PossPOW workshop (2015).

[16] R. Krishna, *Available power estimator,* (2012).

[17] TenneT, *Volume of settled imbalance,* (2016).

[18] TenneT, *Implementation Guide*, Tech. Rep. (TenneT, 2012).

[19] B. C. Ummels, *Power System Operation with Large-Scale Wind Power in Liberalised Environments*, Ph.D. thesis, Delft University of Technology, The Netherlands (2009).

[20] TenneT, *Settlement prices,* (2016).

[21] R. N. E. Agency, *Wind SDE+ 2015 (land, meer en dijk),* (2016).

[22] N. A. Janssens, S. Member, G. Lambin, and N. Bragard, *Active Power Control Strategies of DFIG Wind Turbines,* IEEE Power Tech 2007 , 1 (2007).

[23] T. Burton, N. Jenkins, D. Sharpe, and E. Bossanyi, *Wind Energy Handbook* (John Wiley & Sons, Ltd, 2011) pp. 1–642.

[24] H. A. Madsen, N. N. Sørensen, and S. Schreck, *Yaw aerodynamics analyzed with three codes in comparison with experiment,* ASME 2003 Wind Energy Symposium, WIND2003 , 94 (2003).

[25] D. Medici, *Experimental Studies of Wind Turbine Wakes - Power Optimisation and Meandering*, Tech. Rep. December (Royal Insititue of Technology, Stockhol, Sweden, 2005).

[26] S. Wan, L. Cheng, and X. Sheng, *Effects of Yaw Error on Wind Turbine Running Characteristics Based on the Equivalent Wind Speed Model,* Energies **8**, 6286 (2015).

[27] Martin O. L. Hansen, *Aerodynamics of Wind Turbines, 2nd edition* (Earthscan London, 2008) p. 192.

[28] L. Vermeer, J. Sörensen, and A. Crespo, *Wind turbine wake aerodynamics,* Progress in Aerospace Sciences **39**, 467 (2003).

[29] A. Crespo and J. Hernández, *Turbulence characteristics in wind turbine wakes,* Journal of Wind Engineering and Industrial Aerodynamics **61**, 71 (1996).

[30] N. Troldborg and J. Sørensen, *A simple atmospheric boundary layer model applied to large eddy simulations of wind turbine wakes,* Wind Energy **17**, 657 (2014).

[31] H. Glauert, *Airplane Propellers*, Vol. 4 (Springer, 1935) pp. 169–360.

[32] R. Gómez-Elvira, A. Crespo, E. Migoya, F. Manuel, and J. Hernández, *Anisotropy of turbulence in wind turbine wakes,* Journal of Wind Engineering and Industrial Aerodynamics **93**, 797 (2005).

[33] B. Sanderse, *Aerodynamics of wind turbine wakes: Literature review*, Tech. Rep. October (Delft University of Technology, The Netherlands, 2009).

[34] M. Kloosterman, *Development of the Near Wake behind a Horizontal Axis Wind Turbine,* Masters of science (2009).

[35] F. Holzäpfel, T. Hofbauer, D. Darracq, H. Moet, F. Garnier, and C. F. Gago, *Analysis of wake vortex decay mechanisms in the atmosphere,* Aerospace Science and Technology **7**, 263 (2003).

[36] G. C. Larsen, H. A. Madsen, J. Torben, and N. Troldborg, *Wake modeling and simulation,* Wind Energy **1653**, 1 (2008).

[37] R. J. Barthelmie, S. T. Frandsen, M. N. Nielsen, S. C. Pryor, P. E. Rethore, and H. E. Jørgensen, *Modelling and measurements of power losses and turbulence intensity in wind turbine wakes at middelgrunden offshore wind farm,* Wind Energy **10**, 517 (2007).

[38] D. Baldacchino and G. J. W. van Bussel, *Wind turbine wake stability investigations using a vortex ring modelling approach,* Journal of Physics: Conference Series **555**, 012111 (2014).

[39] M. Liu, M. Yocke, and T. Myers, *Mathematical model for the analysis of wind-turbine wakes,* Journal of Energy **7**, 73 (1983).

[40] G. C. Larsen, H. A. Madsen, K. Thomsen, and T. J. Larsen, *Wake meandering: a pragmatic approach,* Wind Energy **11**, 377 (2008).

[41] G. P. Corten, K. Lindenburg, and P. Schaak, *Assembly of energy flow collectors, such as windpark, and method of operation,* (2007).

[42] J. Wagenaar, L. Machielse, and J. Schepers, *Controlling Wind in ECN's Scaled Wind Farm,* Ewea 2012 , 3 (2012).

[43] J. Serrano González, M. Burgos Payán, J. M. R. Santos, and F. González-Longatt, *A review and recent developments in the optimal wind-turbine micro-siting problem,* Renewable and Sustainable Energy Reviews **30**, 133 (2014).

[44] S. Frandsen, R. Barthelmie, S. Pryor, O. Rathmann, S. Larsen, and J. Hojstrup, *Analytical modelling of wind speed deficit in large offshore wind farms,* Wind Energy **9**, 39 (2006).

[45] L. Sætran, P.-å. Krogstad, and M. S. Adaramola, *Performance and wake development behind two in-line and offset model wind turbines - " Blind test " experiments and calculations,* Journal of Physics: Conference Series **012171** (2014), 10.1088/1742-6596/524/1/012171.

[46] D. J. Renkema, *Validation of wind turbine wake models*, Ph.D. thesis, Delft University of Technology, The Netherlands (2007).

[47] J. Zhang, M. Cheng, Z. Chen, and X. Fu, *Pitch angle control for variable speed wind turbines,* 2008 Third International Conference on Electric Utility Deregulation and Restructuring and Power Technologies , 2691 (2008).

[48] P. Sorensen, N. A. Cutululis, A. Vigueras-Rodriguez, L. E. Jensen, J. Hjerrild, M. H. Donovan, and H. Madsen, *Power Fluctuations From Large Wind Farms,* IEEE Transactions on Power Systems **22**, 958 (2007).

[49] V. G. Mahesh A. Morjaria, *System, device, and method for estimating possible power output of wind turbines,* (2012).

[50] M. S. Thomas Esbensen, Ramakrishnan Krishna, Frank Scheurich, *System for automatic power estimation adjustment,* (2007).

[51] N. O. Jensen, *A note on wind generator interaction*, Tech. Rep. (Risø National laboratory, Roskilde, Denmark, 1983).

[52] J. Choi and M. Shan, *Advancement of Jensen (Park) Wake Model,* European Wind Energy Conference and Exhibition 2013 , 1 (2013).

[53] J. W. V. Heemst, *Improving the Jensen and Larsen Wake Deficit Models*, Ph.D. thesis, Delft University of Technology (2015).

[54] I. Katic, J. Højstrup, and N. Jensen, *A Simple Model for Cluster Efficiency,* European Wind Energy Association Conference and Exhibition , 407 (1986).

[55] J. Ainslie, *Calculating the flowfield in the wake of wind turbines,* Journal of Wind Engineering and Industrial Aerodynamics **27**, 213 (1988).

[56] H. A. Madsen, G. C. Larsen, T. J. Larsen, N. Troldborg, R. Mikkelsen, P. O. Box, and D. Roskilde, *Calibration and Validation of the Dynamic Wake Meandering Model for Implementation in an Aeroelastic Code,* Journal of Solar Energy Engineering **132**, 2 (2009).

[57] O. S. Rathmann, S. T. Frandsen, and M. Nielsen, *Wake Decay Constant for the Infinite Wind Turbine Array,* European Wind Energy Association Conference, EWEA 2010 , 1 (2010).

[58] John Anderson, *Fundamentals of Aerodynamics*, 5th ed., 5th (McGraw-Hill, 2010) arXiv:arXiv:1011.1669v3 .

[59] J. Johansen, N. N. Sørensen, J. a. Michelsen, and S. Schreck, *Detached-Eddy simulation of flow around the NREL phase-VI blade,* ASME 2002 Wind Energy Symposium, WIND2002 , 106 (2002).

[60] P.-Å. Krogstad and L. Sætran, *Wind turbine wake interactions; results from blind tests,* Journal of Physics: Conference Series **625**, 012043 (2015).

[61] a. Jimenez, A. Crespo, E. Migoya, and J. Garcia, *Advances in large-eddy simulation of a wind turbine wake,* Journal of Physics: Conference Series **75**, 012041 (2007).

[62] W. Noordoostpolder, *Windpark Noordoostpolder,* (2016).

[63] R. Lanzafame and M. Messina, *Fluid dynamics wind turbine design: Critical analysis, optimization and application of BEM theory,* Renewable Energy **32**, 2291 (2007).

[64] Lanchester F.W., *Aerodynamics*, 1st ed. (A. Constable & Co., Ltd, London, 1907).

[65] Westermeerwind, *Westermeerwind,* (2016).

[66] N. Westermeerwind Wind Farm, *Westermeerwind Wind Farm, Netherlands,* (2016).

[67] Siemens, *Wind Turbine SWT-3.0-108 / SWT-3.2-108 / SWT-3.4-108,* (2006).

[68] DNV, *OS-J103 - Design of Floating Wind Turbine Structures*, Tech. Rep. June (DNV - GL, 2013).

Note: All references are provided with cyan clickable links to the original files in the digital PDF version of this report.

A

WESTERMEERWIND

This appendix provides a general description and technical details of the Dutch Westermeerwind wind farm. Westermeerwind will be used in the Master thesis as a case study in order to validate the produced theoretical and numerical methodologies. Westermeerwind is a wind farm that contributes to the goal of the Dutch government to generate at least 14% of its electricity from renewable sources by 2020.

The motto of Westermeerwind is that it is *made for the polder, by the polder*. The project was initiated by local farmers and other people from the Noordoostpolder are able to participate financially in the project. It also tries to involve as many local subcontractors as possible. Westermeerwind aims to be a project that excels in the development, construction and management over its 20 year lifetime, contribute to clean energy for people, nature and the environment and obtain a broad support among nearby living people.

All information presented in this appendix is obtained from publicly available information, mostly from the website of Westermeerwind [65], unless indicated otherwise.

A.1. Wind Farm Cluster Windpark Noordoostpolder

Westermeerwind is part of a cluster named *Windpark Noordoostpolder* [62]. It consists of three wind farms placed near each other. The complete cluster consists of 86 wind turbines and has a total estimated production of $1.4 \cdot 10^6 MWh$. This is enough to provide 400,000 house holds with electricity, which is roughly the same amount of house holds as the two neighboring provinces Flevoland and Friesland.

Wind Farm NOP Agrowind & Zuidwester

Two of these wind farms (i.e. NOP Agrowind and Zuidwester) are offshore projects placed just behind the dike that protects the polder[1] Noordoostpolder from the lake IJsselmeer.

[1] *"A polder is a piece of low-lying land reclaimed from the sea or a river and protected by dykes, especially in the Netherlands."* (Oxford Dictionaries) The Noordoostpolder was completely reclaimed from the - at that time - sea in 1942.

A

These two wind farms visually form a single segmented line of 38 turbines (of the same type) along this dike, but have different owners, see figure A.1. These turbines are of the type Enercon E-126 7.58MW.

Wind Farm Westermeerwind

Wind farm Westermeerwind itself consists of 48 Siemens Wind Power 3.0MW D3-108 wind turbines placed near shore, leading to a total rated power of 144MW. This is enough to provide 160,000 house holds of electricity. A wind farm was installed at the same location of the wind farm cluster consisting of 50 wind turbines 25 years ago. However, just two of the new 3.0MW turbines produce more energy per year than this old wind farm. A sign of a maturing industry.

Ventolines BV

The total project management is outsourced to company Ventolines BV, which is also a partner of this project. Ventolines is a full service provider in wind energy. It provides services in all stages of wind energy projects of all sizes: development, financing, contracting, implementation and management.

Partners

The total funding of the project is €320M, which is provided by Dutch banks and party guaranteed by a Danish export credit agency. The power produced by Westermeerwind is bought by Dutch electricity supplier Eneco under a PPA for 15 years. Siemens has the responsibility of the completion of the project by a turnkey contract, including 15 year of maintenance. Subcontractors are Ballast Nedam and Mammoet for the foundation installation and turbine transportation and installation, respectively. Visser & Smit Marine Contracting will install the cables to the onshore electrical substation. [66]

A.2. Wind Farm layout

As can be seen in figure A.1, Westermeerwind consists of two parts. The Northern part at the dike *Noordermeerdijk*, is single row of 13 turbines where the turbines have a spacing of 520m (5D). The Soutern part at the dike *Westermeerdijk*, are two rows of 17 and 18 turbines, with a spacing of 416m (4D). The wind farm is located near shore, 1100m (Noordermeerdijk) and 500m (Westermeerdijk) outside of the polder. The water depth ranges from 3m to 7m.

A.3. Wind Turbines

The three bladed turbines from Siemens Wind Power have a permanent magnet direct drive generator with a rated capacity of 3MW and a rotor diameter of 108m. It is a pitch regulated turbine, but also allows variable rotational speed. It is installed at Westermeerwind with a hub height at 95m and a tip height of 149m. The turbines are mounted on monopiles with a diameter of 5m and a length of 40m. [66]

The 53m long blades are innovative in their aero-elastic design allowing higher energy outputs and reducing the cost of energy. They are made from fiberglass-reinforced epoxy. The reader is referred to the website of the turbine for the full specifications. [67]

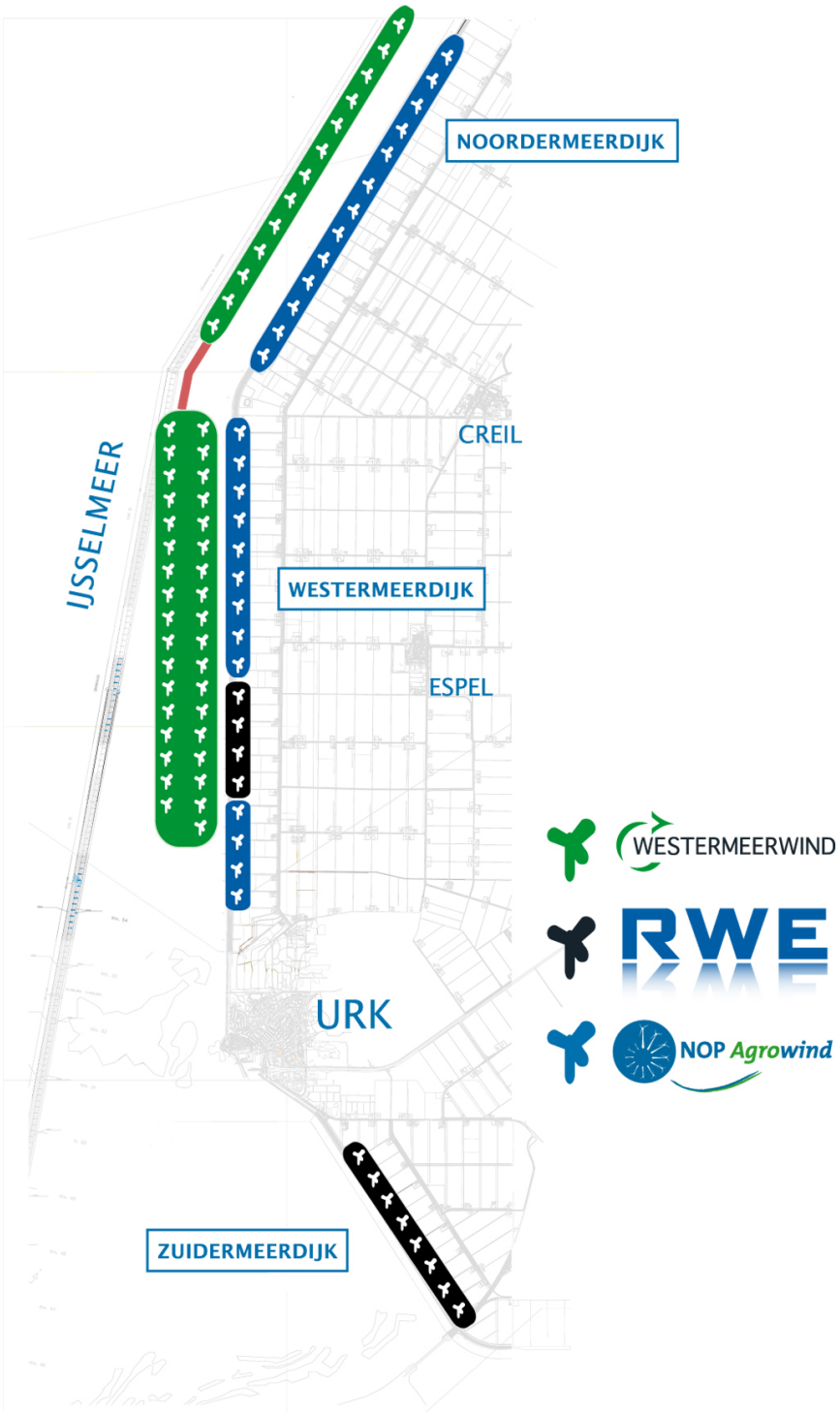

Figure A.1: Wind farm cluster *Windpark Noordoostpolder*. The green marked wind turbines are part of the wind farm Westermeerwind related to this report[62]

B

WIND TURBINE FUNDAMENTALS

This appendix serves as a fundamental basis for chapter 3. It provides the knowledge to understand where the wakes originate from, namely the wind turbine itself. As wind turbine design integrates many different disciplines, a selection of its fundamentals is made. First, the most important graphs describing a wind turbine are discussed. Second, all relevant aerodynamics of the rotor are presented in order to derive the momentum theory, which leads to the Betz limit. Also a short description of a fundamental rotor design algorithm, called the Blade Element Momentum method is presented.

B.1. Power Curve

When a new wind farm is designed, the selection of the right wind turbine is essential. The designer wants to extract as much energy from the wind as possible, in order to increase the profits of the wind farm. The amount of energy a turbine can extract from the wind is mainly dependent on two factors. First, the wind conditions of the specific site need to be known. When the wind speed is high, a different turbine (maybe larger or different blades) is required than when the wind speeds are low. Second, the characteristics of the turbine need to be compatible with the site conditions. When the wind speed of the site stays within a small band, it might be favorable to select a turbine that specializes on that band.

Figure B.1 shows an example of a power curve for two types of power control. The solid line shows the power curve for stall control of the turbine. Stall control means that the individual blades of the rotor are unable to pitch. They have a fixed pitch angle and are aerodynamically designed to generate a torque that keeps the power below rated power at higher wind speeds. The dashed lines displays an active pitch controlled wind turbine. As the latter is more common for larger turbines, only this type of turbine is considered in this report.

There are several points in figure B.1 that need attention. First, the power curve does not start at the origin, but only at $4\frac{m}{s}$. This wind speed is referred to as the cut-in wind speed. A lower value of the cut-in wind speed, means that the turbine is able to operate

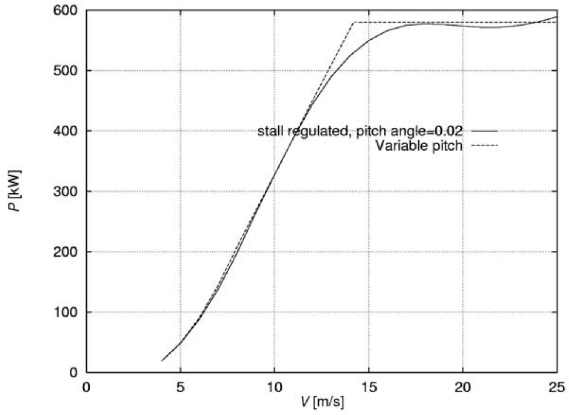

Figure B.1: Power Curve for the NTK 500/41 wind turbine for both stall and pitch control [27]

at lower wind speeds and is therefore a more favorable option for sites with low wind conditions.

Second, the sharp corner at $14\frac{m}{s}$ is the point where the turbine reaches its maximum (or rated) power. It is therefore referred to as the rated wind speed. At wind speeds lower than this the curve follows equation B.1, which will be proven in section B.2. In this equation V_0 is the incoming wind speed, A the swept area of the rotor, ρ the density of the air and C_P the power coefficient, which will be treated later. At wind speeds higher than this, the production of turbine has to be lowered to the rated power otherwise the generator will overheat and break. This is done by reducing the efficiency of the blades by pitching them to a non-optimal working point.

$$P = \frac{1}{2}\rho V_0^3 A C_p \tag{B.1}$$

There are two options when the blades is pitched for power reduction. These are pitch to stall and pitch to feather, corresponding to the two directions the blades can be rotated to. Figure B.2 shows two graphs. In the left graph the effect of rotating (pitching) the blades can be seen. For higher or lower values of the pitch angle than zero, the power curve moves to the right. One could observe that a non-zero pitch angle is more efficient, as the peaks are higher, but at the sub-rated wind speeds the power curve of the zero pitch angle is actually the highest. However, in most cases pitch to feather is used. The most important reason is that during this type of pitching, the flow stays attached to the blade and is therefore better understood than stalled flow. The risk and predictability of pitching to feather are therefore lower than pitching to stall. Also, because the flow is still attached during feather, the rotor provides better aerodynamic damping than stalled conditions. A drawback of feathering is, however, that the turbine is more sensitive to wind gusts. Sudden increasing wind speeds can therefore lead to big increases in the torque on the generator - observe the steep curves of the power curve corresponding to $+4°$ at $12\frac{m}{s}$. The right graph of figure B.2 shows how the rated part of the power curve is constructed. Below rated velocity the pitch angle is kept at zero degrees. As soon as

the wind speed hits this point, the pitch angle is increased to feather. Multiple partial power curves have been drawn for different pitch angles. Only the parts crossing the final power curve are shown.

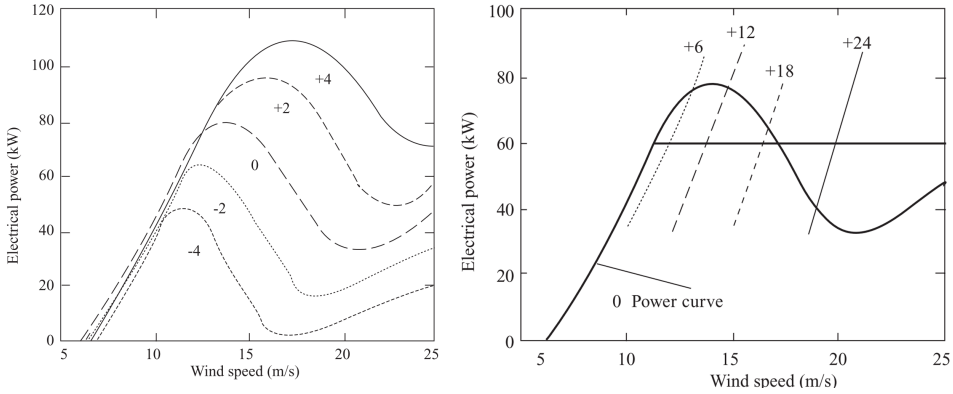

Figure B.2: Effect of pitch angle on the power curve. Positive pitch angle lead to feathered conditions, while negative pitch angles cause blade stall. [23]

The third interesting point is at $25\frac{m}{s}$. The power curve does not continue, but it reaches its end. The process of pitching is continued until the wind speed hits a predefined cut-out wind speed. The wind turbine is then brought to a full stop. In this phase, the turbine is often pitched to stall, to avoid the sensitivity to wind gusts as mentioned before. [23]

B.2. Aerodynamics of the Momentum Theory

This section provides the necessary knowledge of aerodynamics to understand why wakes occur. The goal is to derive the momentum theory, which forms the basis of wind turbine analysis and design.

The momentum theory is the basis for the Blade Element Momentum (BEM) method, which couples this theory to the actual blade design, e.g. the airfoil, the twist angle and chord distribution and the number of blades. This allows the calculation of actual power and thrust curves of a specific turbine design. Although many wind turbine manufactures have created their own advanced and complex implementation of the BEM method, they all originate from the momentum theory. [68] Section B.4 will provide more information about this method.

Assumptions

This derivation is a summary taken from [27] and the reader is reffered to this reference for the full derivation. The following assumptions are made. First, it considers the rotor as an ideal disk, e.g. there it is assumed frictionless and zero rotation in the wake. Section B.3 will discuss Glauerts correction for the latter relevant with respect to the BEM and section 3.1.2 will completely disregard this assumption and look into the effects of vorticity. Second, the flow is assumed to be stationary, incompressible (low Mach num-

ber), uniform, frictionless and no external forces act on the fluid. Especially the last flow assumption is invalid for far wake analyses, as when the wake expands the ground will act as a fixed expansion boundary. Section 3.1.4 will provide corrections for this assumption. Section 3.1.4 will invalidate the assumption of uniform flow and introduce the so called wind shear.

Actuator Disk Theory

The momentum theory is also called the actuator disk theory, as it describes a mathematical model of the rotor as seen as an ideal actuator disk. Treating the disk as a drag device, the wind is slowed down from V_0 upstream via u at the disk to u_1 in the far wake. Because of this reduction in wind speed, the streamlines of the incoming wind have to diverge as a result of the law of conservation of mass, see figure B.3.

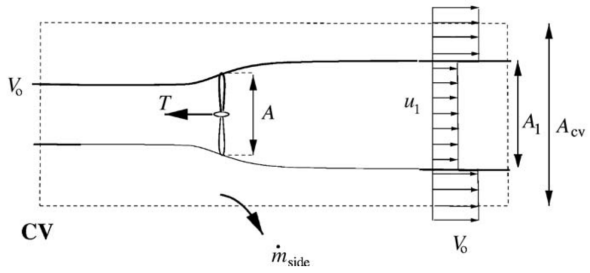

Figure B.3: Expansion of the streamlines with out of plane circular area $A = \pi R^2_{rotor}$ [27]

The pressure, however, increases when the air approaches the wind turbine. Across the rotor the pressure decreases suddenly, but gradually goes back to atmospheric pressure. Because of the flow assumptions, Bernoulli can be applied along these stream lines (except over the pressure drop itself), resulting in an expression for the pressure drop in figure B.4.

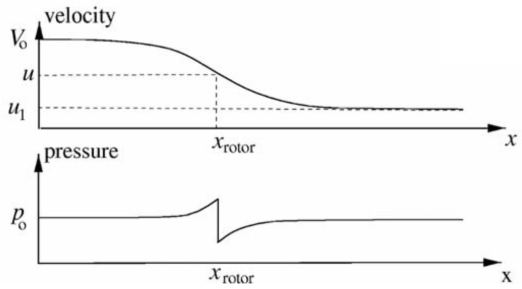

Figure B.4: Pressure and velocity upstream and downstream of the rotor [27]

$$\begin{cases} p_0 + \frac{1}{2}\rho V_0^2 = p + \frac{1}{2}\rho u^2 & before\ disk \\ p - \Delta p + \frac{1}{2}\rho u^2 = p_0 + \frac{1}{2}\rho u_1^2 & after\ disk \end{cases} \rightarrow \Delta p = \frac{1}{2}\rho(V_0^2 - u_1^2) \tag{B.2}$$

This pressure drop can be used to calculate the thrust force on the rotor as in equation B.3.

$$T = \Delta p A = \frac{1}{2}\rho A(V_0^2 - u_1^2) \tag{B.3}$$

The Momentum Equation

The control volume for the expression of the momentum integral is shown in figure B.3, resulting in the equation B.4.

$$\frac{\partial}{\partial t}\iiint_{cv} \rho u(x,y,z)dxdydz + \iint_{cv} u(x,y,z)\rho\vec{V}\cdot\vec{dA} = F_{external} + F_{pressure} \tag{B.4}$$

The terms $F_{external}$ and $F_{pressure}$ represent external force and the axial component of the pressure force on the control volume, respectively. The former term is assumed to be zero as a result of the assumption of stationary flow and the later is zero since the same atmospheric pressure acts on both sides of the control volume. Equation B.4 can further be simplified to equation B.5 by taking into account that there is no axial component of the pressure force along the lateral boundary.

$$\rho u_1^2 A_1 + \rho V_0^2 (A_{cv} - A_1) + \dot{m}_{side} V_0 - \rho V_0^2 A_{cv} = -T \tag{B.5}$$

Conservation of Mass

Using the principle of the conservation of mass over the all boundaries of the control volume as in equation B.6, the expression for the thrust force T can be obtained as in equation B.7.

$$\begin{aligned} &\dot{m}_{right} + \dot{m}_{up\&down} = \dot{m}_{left} \\ &\rightarrow \left\{\rho A_1 u_1 + \rho\,(A_{cv} - A_1)\,V_0\right\} + \dot{m}_{side} = \rho A_{cv} V_0 \\ &\rightarrow \dot{m}_{side} = \rho A_1 (V_0 - u_1) \end{aligned} \tag{B.6}$$

$$T = \rho u A(V_0 - u_1) = \dot{m}(V_0 - u_1) \quad with \quad \dot{m} = \rho u A \tag{B.7}$$

Comparing the expressions of the thrust force from equation B.3 and B.7, results in an interesting expression of the wind speed u. The wind speed at the rotor appears to be the average of the incoming wind speed and the wake wind speed.

$$\begin{aligned} &\rho u A(V_0 - u_1) = \tfrac{1}{2}\rho A(V_0^2 - u_1^2) \\ &\rightarrow u(V_0 - u_1) = \tfrac{1}{2}(V_0^2 - u_1^2) \\ &\rightarrow u = \tfrac{1}{2}(V_0 + u_1) \end{aligned} \tag{B.8}$$

Axial Induction Factor

One final reformulation is made to this expression by introducing the (axial) induction factor a, as defined in equation B.9. The induction factor describes the ratio of the wind speed at the rotor with respect to the free-stream wind speed.

$$a = 1 - \frac{u}{V_0} \tag{B.9}$$

Later, also the tangential induction factor will be used as in equation B.10.

$$a' = \frac{u_t}{\omega r} \tag{B.10}$$

Using the axial induction factor, wind speeds u and u_1 can be rewritten as in equation B.11.

$$\begin{aligned} u &= (1-a)V_0 \\ u_1 &= (1-2a)V_0 \end{aligned} \tag{B.11}$$

Shaft Power

If the control volume is taken along the outer streamlines from figure B.3 instead, the expression of the internal energy can be used to calculate the shaft power P. Here the assumption of the frictionless flow is implemented.

$$\frac{P_{shaft}}{\dot{m}} = \frac{1}{2}V_0^2 + \frac{p_0}{\rho} - \frac{1}{2}u_1^2 - \frac{p_0}{\rho} + f_{friction} \tag{B.12}$$

Using the same expression for $\dot{m}$ as in equation B.7, the shaft power can be found as in equation B.13.

$$P_{shaft} = \frac{1}{2}\rho u A(V_0^2 - u_1^2) \tag{B.13}$$

Equation B.13 can be rewritten to include the induction factor. This leads to equation B.14, which forms the basis of the theory for the Betz limit. The next section will go into more detail on this limit. An important observation from equation B.14 is that the shaft power of the wind turbine depends on the free-stream wind speed with a power factor 3. This again shows the importance for an accurate description of the wind speed in order to calculate the available wind power (whether or not during curtailment).

$$P_{shaft} = 2\rho V_0^3 A a(1-a)^2 = \frac{1}{2}\rho V_0^3 A C_p \tag{B.14}$$

B.3. The Betz Limit

In 1920, Albert Betz introduced a law that describes the upper limit of the efficiency of a wind turbine. This limit is known as the Betz limit and it is independent on the design of the wind turbine, making it very usefull as a benchmark for wind turbines. Betz (and debatably also Joukowsky and Lanchester), used the actuator disc theory of section B.2 as a basis of his theory.

The result of his theory, e.g. equation B.14, is shown in figure B.5, based. It shows the power coefficient of the turbine with respect to the wind speed deficit a. This speed deficit is defined as the ratio between the wind speed before and after the rotor. If a would be 1.0, the fluid would come to a complete stop just behind the turbine. This

blockage would in turn make it impossible for new fluid to flow through the rotor, resulting in a total drop of torque on the rotor. Therefore, the maximum efficiency has to be below $a = 1.0$ and can indeed be found as $C_p(\frac{1}{3}) = 16/27 \approx 59.3\%$.

$$C_p(a) = 4a(1-a)^2 \tag{B.15}$$

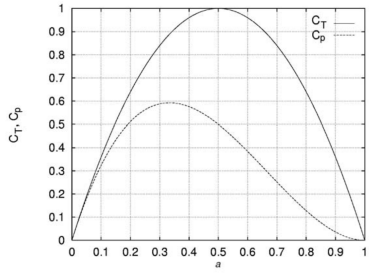

Figure B.5: The power and thrust coefficient against the induction factor (equation B.15) [27]

It can be concluded from Betz' theory that a wake is not only unavoidable, but a wake with a deficit ratio of $a = \frac{1}{3}$ is even desired for optimal performance. It has to be noted, however, that this describes the performance of an individual turbine, which is not necessarily equal to the complete wind farm performance. Section 3.2 will go more in to depth about this discrepancy.

A second note is that the Betz limit is derived for zero rotation in the wake. Glauert calculated a corrected optimum for the power coefficient for different tip speed ratios λ (see equation 3.8) as shown in figure B.6. Section 3.1.2 will go more into depth about the rotation of the wake.

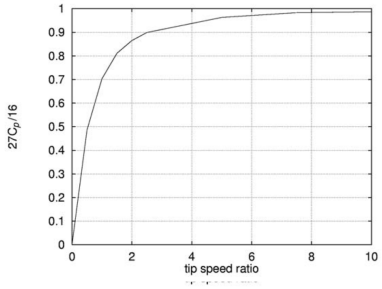

Figure B.6: Glauerts optimum power coefficient with respect to the Betz limit ($\frac{16}{27}$) against the tip speed ratio.

B.4. Blade Element Momentum Method

Although mostly outside the scope of this report, a short description of the Blade Element Momentum (BEM) method is presented, as it is a crucial and fundamental theory

wind turbine design. It was presented by Glauert [31] and consists of an iterative code, that can be summarized into the following eight steps.

1. Initialize a and a' (typically $a = a' = 0$), where a is the axial induction factor and a' is the tangential induction factor. These parameters need to be set as an input for the iteration loop. Sometimes a value of $a = \frac{1}{3}$ increases convergence time.
2. Compute the flow angle ϕ, using $\tan(\phi) = \frac{(1-a)V_0}{(1+a')\omega r}$ The flow angle is the angle between the relative velocity (taking radial velocity into account together with free stream velocity) and the rotor plane, see figure B.7.
3. Compute the local angle of attack, using $\alpha = \phi - \theta$, where θ is the local twist angle.
4. Get lift and drag coefficient from drag polar of respective airfoil.
5. Compute normal and tangential coefficients, using $C_n = C_l \cos(\phi) + C_d \sin(\phi)$ and $C_t = C_l \sin(\phi) - C_d \cos(\phi)$.
6. Calculate a and a' from $a = \frac{1}{\frac{4\sin^2(\phi)}{\sigma C_n}+1}$ and $a' = \frac{1}{\frac{4\sin(\phi)\cos(\phi)}{\sigma C_t}+1}$, where $\sigma = \frac{cB}{2\pi r}$ is the annular area covered by the blades with chord c.
7. If a and a' have changed more than a certain tolerance, go back to step 2, using the current values of a and a' as an input.
8. Calculate the local load at the segments of the blades, using the calculated force coefficients C_l and C_d or C_n and C_t.

For the full derivation of all these equations, the reader is referred to [27]. The goal here is to show all the inputs the BEM method deals with:

- V_0 Free stream wind speed
- ω Radial velocity
- r Rotor radius
- θ Local twist angle
- C_l and C_d Drag polar airfoil
- c Local chord
- B Amount of blades

Although this method is relatively easy, in order to get more accurate results corrections should be applied. This is where wind turbine manufacturers can distinguish themselves. The following two corrections are always necessary. The first is called Prandtl's tip loss correction, which accounts for the assumption of an infinite number of blades. The second correction is called the Glauert correction and provides a solution for the region where a is larger than 0.4. In this region u_1 will become negative when using equation B.11, which is incorrect. The reader is referred to [27] and [63] for its implementation in the eight step algorithm above.

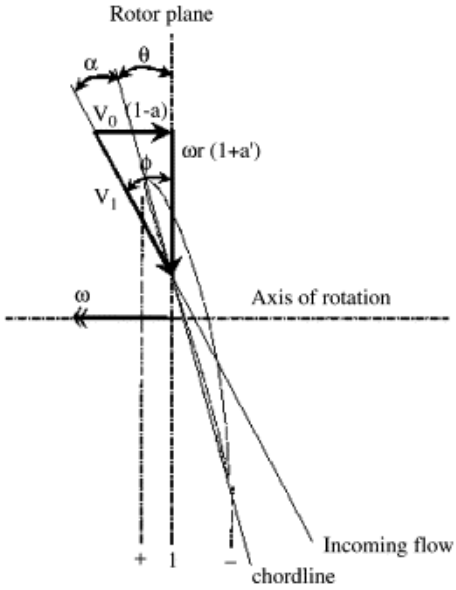

Figure B.7: Angles, velocities and induction factor for the BEM method [63]

B.5. Aerodynamics of an Airfoil

In the previous sections the vorticity has been disregarded as is has a relatively low influence on individual turbine design. However, when considering the interference between turbines, vorticity plays a very important role as discussed in section 3.1 about wake fundamentals. But, before the wake fundamentals can be studied, more knowledge is required about vortex creation on a low aerodynamic level. First, the aerodynamic definition of vortex flow is defined. Second, the creation of vortex flow is explained.

Vortex Flow

Vortex flow is a type of flow where all its streamlines are concentric circles as seen in figure B.8. The velocity along a streamline is constant, but can change with radial distance from the centre, as in equation B.16. Γ is called the strength of the vortex flow or the circulation of the vortex flow. [58].

$$V_\theta = -\frac{\Gamma}{2\pi r} \tag{B.16}$$

Flow Separation

The first source of vortex flow is due to flow separation. This occurs when the angle of attack of the airfoil is increased to such a high value, that the fluid will not stick to the airfoil anymore, but detaches as in figure B.9. The point of separation will move forward from the trailing edge to the leading edge with an increase in angle of attack. In the most right graph of figure B.9 these detached flow lines can be observed. As the wake behind

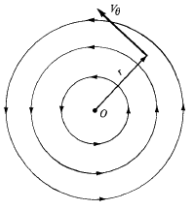

Figure B.8: Elementary Vortex Flow [58]

the airfoil has a very low wind speed, but the continuous flow lines have a relative high wind speed, rotation of the air will occur. This rotation is very unpredictable as it highly depends on small defects in the incoming wind. Therefore, in contrary to the attached laminar flow, this turbulent flow is a very random and contains many defects itself.

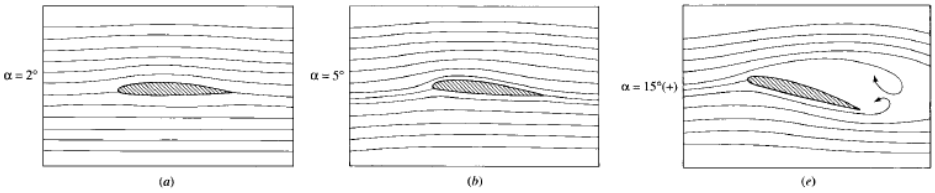

Figure B.9: Flow Separation [58]

An important note has to be made, that during the constant power output regime, described in section B.1, the control mechanism is (most often) pitch control, see section 2.3. During pitch control, the angle of attack is increased to lower the torque on the generator. The process of vortex generation due to flow separation is therefore an important phenomenon for wind turbines.

Tip Vortex

A second source of vortex generation is the difference in pressure at the tip of the blade. It is a result of Lanchester's theory on finite wings. When looking at a wing of an airplane, the higher pressure below the wing causes air to flow from under to wing to the lower pressure area above the wing, see figure B.10. The same forces act on a blade of a wind turbine, but rotate around the axis of the rotor, see figure 3.9.

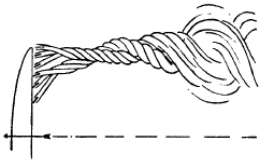

Figure B.10: Wing tip vortex of finite wing (airplane) [64]